UNIVERSIDADE DA BEIRA INTERIOR
Ciências da Saúde

Design and production of new nanodevices for future application in cancer therapy

Ana Sofia Matias da Silva

Thesis dissertation for MsC in Master degree thesis
Biomedical Sciences
(2nd cycle of studies)

Supervisor: Ilídio Correia, PhD

Covilhã, June 2011

UNIVERSIDADE DA BEIRA INTERIOR
Ciências da Saúde

Desenho e produção de novos nanodispositivos para futura aplicação na terapia do cancro

Ana Sofia Matias da Silva

Dissertação para obtenção do Grau de Mestre em
Ciências Biomédicas
(2º ciclo de estudos)

Orientador: Prof. Doutor Ilídio Correia

Covilhã, Junho de 2011

"Tenho pensamentos que, se pudesse revelá-los e fazê-los viver,acrescentariam nova luminosidade às estrelas, nova beleza ao mundo e maior amor ao coração dos homens". **Fernando Pessoa**

Dedication

I would like to dedicate this Master Thesis to two of the most important people that ever crossed my life: my Grandmother Deolinda and my 'second' father Fernando. Because I know that both of you would like to be next to me in this moment of my life and because I do believe that in 'Every step I take, you'll be watching me'.

Acknowledgments

I would like to thank my supervisor Professor Ilídio Correia for the unconditional support, guidance and help during my master's degree. Specially, I feel the need to acknowledge him for having believed in my capabilities and for making me believe in myself. It has been a privilege working with him.

Furthermore, I would like to thank Professor António Mendonça for all the help and for the recipe to produce gold nanoparticles.

I also acknowledge to Professor Ana Aguiar and Professor Vasco Bonifácio from the Universidade Nova de Lisboa, for providing us oligoaziridine biosensor and for the support to continue this project.

Moreover, I would like to thank to Eng. Ana Paula from the Optics department of Universidade da Beira Interior for the help in acquiring scanning electron microscopy images of the nanoparticles produced.

I would also like to thank to Dr. Catarina Ferreira for the help in the acquisition of immunofluorescence and confocal laser microscopy images.

In addition, I would like to thank to all of my group colleagues for all the teaching, for having supported me whenever I was feeling down, for all the laughs that made me feel good and for all the experience shared during these months. Their friendship was, without any doubt, very important to overcome the difficulties faced.

From the bottom of my heart I thank to my family and closest friends, from the youngest to the elderly for the love, support and patience not only during the execution of this master thesis, but also through my entire academic course. They were truly important in all of my victories and they are definitely 'the only love that doesn't make me weak'.

I could not end these acknowledgments without a special thanks to my boyfriend for having appeared in my life when I needed the most. For all the love, support, care and patience during the good and the bad days and for all the advices, I do thank him a lot. Specially, I thank him for having shown me that I'm an amazing woman who deserves to be loved.

Finally, thank you God for…Everything.

Abstract

Nanotechnology is a multidisciplinary area of research that involves different knowledgements from, like life sciences, engineering and medicine. It has been used for different applications such as molecular imaging, molecular diagnosis and also targeted therapy. So far, ddifferent nanoscale devices have been produced, among them, inorganic nanoparticles, dendrimes, lipossomes, polymeric micelles, polymeric nanoparticles, nanotubes and nanofibers are some of the examples. Some of these particles exhibit unique optical and electrical properties allowing their course identification and precise location in the body. Gold nanoparticles are an example of inorganic particles with exceptional physico-chemical properties that demonstrate a huge potential for biomedicine applications.

The present study aimed to produce gold nanoparticles by two different methods: the citrate reduction method developed by Frens in 1973 (method 1), and its functionalization with oligoaziridine, developed by the colleagues from Universidade Nova de Lisboa, as a capping agent (method 2). This second method relies on the fact that gold nanoparticles can be prepared in water directly by the complexation of the alkylamine molecules that act as reducing agents and consequently stabilizes gold nanoparticles.

Moreover, gold nanoparticles produced by method 1 were also grafted with homofunctional maleimide poly(ethylene glycol) and then capped with oligoaziridine and the same parameters mentioned above were also evaluated.

The cytotoxicity and cell internalization of the different nanoparticles herein produced, was evaluated through in vitro studies.

The use of this new biosensor allow us to confirm the entry of the produced nanoparticles into cells opening new sights for the use of these particles as drug/gene delivery agents and/or as a new method for optimal imaging when methodologies like X-ray computed tomography or magnetic resonance cannot be used.

Keywords

Nanotechnology; Gold nanoparticles; Oligoaziridine; Homofunctional Maleimide Poly(ethylene glycol)

Resumo

A nanotecnologia é uma área de investigação multidisciplinar que abrange conhecimentos das ciências da vida, da engenharia e da medicina. Esta área do conheciemnto tem contribuido para melhorar as tecnologias de imagiologia, diagnóstico molecular e na terapia direccionada. Nos últimos anos têm sido produzidos diferentes dispositivos à nanoescala, entre eles destacam-se as nanopartículas inorgânicas, dendrímeros, lipossomas, micelas poliméricas, nanopartículas poliméricas, nanotubos e nanofibras. As nanopartículas de ouro são um exemplo de partículas inorgânicas, e apresentam propriedades físicas e químicas excepcionais que lhe conferem um elevado potencial para aplicações biomédicas.

O presente estudo teve como objectivo produzir nanopartículas de ouro por dois métodos diferentes: o método de redução de citrato desenvolvido por Frens em 1973 (método 1); e o da funcionalização das aminas através da adição de oligoaziridina, um biosensor desenvolvido pelos colegas da Universidade Nova de Lisboa, como agente de revestimento (método 2). Este segundo método envolve a preparação das nanopartículas de ouro directamente em água através da complexação com moléculas acilaminas, que actuam como agentes redutores, estabilizando as nanopartículas de ouro.

Numa segunda fase, as nanopartículas de ouro produzidas pelo método 1 foram revestidas com polietilenoglicol maleimida homofuncional e, em seguida, adiciounou-se oligoaziridine. A citoxicidade e a capacidade de entrarem nas células foi tambem avaliada para estas nanopartículas. Os resultados obtidos demonstram que o polimero polietilenoglicol maleimida homofuncional se liga de uma forma efectiva às nanopartículas de ouro. Por outro lado, provou-se que o oligoaziridine se liga tanto ao polietilenoglicol como às nanopartículas isoladas.

Após a sintese das nanopartículas pelos dois métodos foi avaliada a sua toxicidade e a capacidade de entrarem nas células eucarióticas.

A utilização deste novo biosensor permite confirmar a entrada das nanopartículas nas células, o que possibilitará o uso destas partículas como agentes de entrega direccionada de fármacos, genes ou como um novo método para a obtenção de imagens quando metodologias como Tomografia Computadorizada por raios X ou Ressonância Magnética não poderem ser usadas.

Palavras-chave

Nanotecnologia; Nanopartículas de ouro, Oligoaziridine, Polietilenoglicol Maleimida Homofuncional

Index

List of Figures

Chapter I – Introduction

Chapter III – Results and Discussion

List of Tables

List of Acronyms

ABC	ATP Binding Cassette transporters
ATP	Adenosine Triphosphate
Au_Oligo	Gold nanoparticles produced by method 1 capped with oligoaziridine
AuNP's	Gold nanoparticles
AuNP's_F	Gold nanoparticles produced by method 1
AuNP's_PEG	Gold nanoparticles (produced by method 1) capped with MAL-PEG-MAL
AuNP's_PEG_Oligo	Gold nanoparticles (produced by method 1) capped with MAL-PEG-MAL and Oligoaziridine
CEA	Carcinoembryonic Antigen
CLSM	Confocal Laser Scan Microscopy
EGF	Epidermal Growth Factor
EPR	Enhanced Permeability and Retention effect
ErbB2	Human Epidermal Growth Factor receptor 2
EtOH	Ethanol
FBS	Fetal Bovine Serum
FDA	Food and Drug Administration
Frs	Folate receptors
FTIR	Fourier Transform Infrared
K^-	Negative control
K^+	Positive control
mAB	Monoclonal Antibody
MAL-PEG-MAL	Maleimide-PEG-Maleimide
MDR	Multidrug Resistance
MPS	Mononuclear phagocytic system
MR	Magnetic ressonance
MRI	Magnetic Resonance Imaging
MTS	3-(4,5-dimethylthiazol-2-yl)-5-(3-carboxymethoxyphenyl)-2-(4-sulfophenyl)-2H-tetrazolium
$NaBH_4$	Sodium Borohydride
NIR	Near-Infrared
NLS	Nuclear Location Signal
OLA	Oleyl amine
OligoNP's	Gold nanoparticles produced by method 2
PAAm	Poly(acrylamide)
PAMAM	Polyamidoamine
PBS	Phosphate-Buffered Saline
PEG	Poly(ethylene glycol)
PEG:AuNP's	Poly(ethylene)glycol: Gold nanoparticles ratio
PEG-b-PPO-b-PEG	Poly(ethylene glycol)-b-poly(propylene oxide)-b-poly(ethylene glycol)
PHSRN	Proline – Histidine – Seronine – Arginine – Asparagine
PMS	Phenazine Methosulfate
pNIPAAM	Poly(N-isopropylacrylamide)
PPE	Palmar-plantar erythrodyesthesia
Pr_b	Fibronetic-mimic peptide
PTT	Photothermal Therapy

PVA	Poly(vinyl alcohol)
RGD	Arginine – Glycine – Aspartic acid
SEM	Scanning Electron Microscopy
SPR	Surface Plasmon Resonance
TEM	Transmission Electron Microscopy
Tf	Transferrin
TFrS	Transferrin receptors
UV-VIS	Ultraviolet-Visible
VEGF	Vascular endothelial growth factor
X Ray TC	X ray Computed Tomography
YIGSR	Tyrosine – Isoleucine - Glycine – Seronine – Arginine
YIGSR-NPS	YIGSR attached to nanoparticles surface

Chapter I - Introduction

1. Introduction

1.1. Cancer – A brief discussion of the disease

Cancer is the leading cause of death worldwide accounting for 7.9 million of deaths in 2007 (Dong and Mumper 2010) and World Wide Health Organization predicts that in the year of 2030 this value will rise up to 20 million (Bode & Z. Dong 2009). Cancer may develop from different cell types in the human body and is characterized by relatively uncontrolled proliferation of cells that can invade healthy tissues and metastasize into remote organs (Stratton *et al.,* 2009). The first insights in cancer development emerged in the late 19th and early 20th centuries through the examination of cancer cells by optical microscopy (Stratton *et al.,* 2009). Later on, the observation of peculiar chromosomal aberrations led to the proposal that cancer are abnormal clones of cells, that appear due to the occurrence of modifications in the hereditary material (Stratton *et al.,* 2009). Natural selection, acting on the resulting phenotypic diversity, eliminates cells which have acquired deleterious mutations and foster the ones that have acquired proliferation capabilities (cancer cells) (figure 1) (Visvader and Lindeman 2008; Stratton *et al.,* 2009).

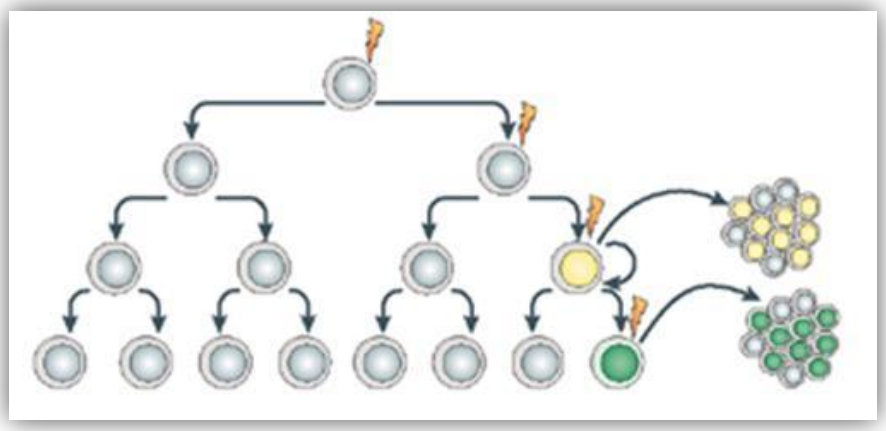

Figure 1 - Cancer evolutive model. All cells possess similar tumorigenic capacity. Mutant tumor cells with growth advantage prevail over normal cell types thus increasing tumorigenic tissue (Adapted from Visvader and Lindeman 2008).

Nevertheless, cancer development is accepted as a multistep process, during which genetic alterations promote abnormal cell growth, which leads to the progressive transformation of normal and healthy cells into to cancer ones (Hanahan 2000). Figure 2 summarizes the key event changes that characterize the appearance and growth of a cancer cell.

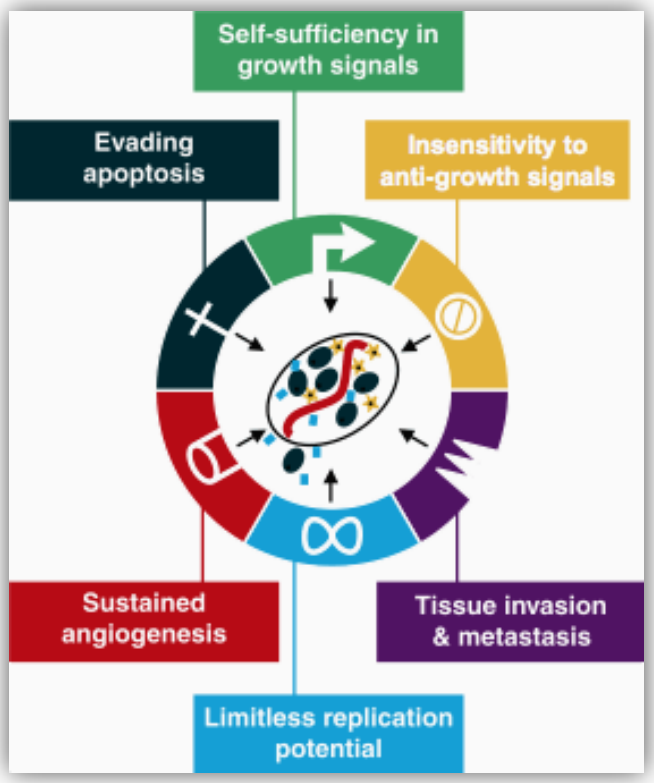

Figure 2 – Illustration of the metabolic changes that occur in cancer cells. Malignant growth is characterized by several key events as self-sufficiency in growth signals, insensitivity to anti-growth signals, cell avoids apoptosis, deregulated proliferation potential, enhanced angiogenesis, ability to invade tissues and metastasize. (Adapted from Hanahan 2000)

1.1.1. Events that lead to cancer disease

The genetic alterations in cancer must be understood in a context of cellular organization, differentiation, tissue organization, host response and susceptibility to angiogenesis. Several factors can influence the evolution of a cancer, like different events that occur inside of the cell (as gain or loss of function events), epigenetic events, environmental exposures (e.g., radiations or smoke), systemic effects like hormones or growth factors and paracrine interactions with neighbouring cells (figure 3) (Hanahan 2000; Ponder 2001).

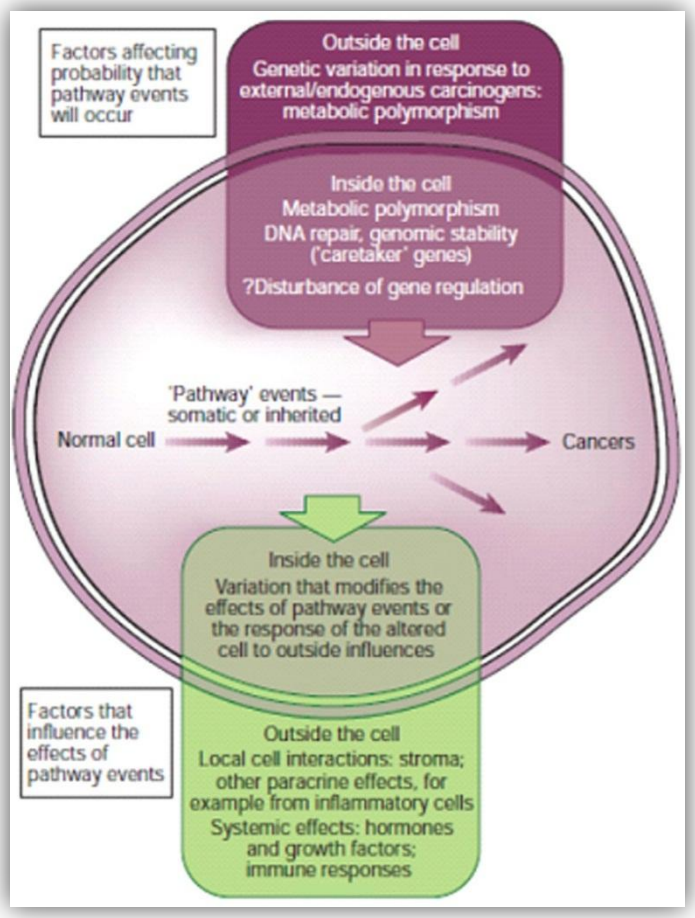

Figure 3 – Framework of genetic events on cancer development. Horizontal arrows represent the pathway of successive genetic or epigenetic events through which the cell may acquire the cancer phenotype. Vertical arrows indicate the influences in this pathway that affect the probability of a specific event to occur (Adapted from Ponder 2001).

The three major classes of genes in which genetic variations occur and subsequently cancer cells arise are oncogenes, tumor suppressor genes, and caretaker genes (Vogelstein and Kinzler 2004). Oncogenes encode proteins that control cell proliferation, apoptose or both. These types of genes can be activated by structural modifications that result from either mutations or gene fusion, or by juxtaposition to enhancer elements (Croce 2008). Mutations in this type of genes are usually associated with gain of function events, i.e., events that confer enhanced activity to the expressed proteins (Collins 1997). Tumor suppressor genes or anti-oncogenes regulate cell division. This type of genes reduces the probability of the cell, in a certain multicellular organism, becomes a tumorigenic one. Mutations in tumor suppressor genes cause a loss or reduction in its function, leading a malignant cell to progress to cancer (Ponder 2001; Vogelstein and Kinzler 2004).

Inactivation of caretaker genes (genes that control genomic integrity) leads to genomic instability and thus contributes for the increase of the probability of alterations in the oncogenes and in the tumor suppressor genes (Ponder 2001; Vogelstein and Kinzler 2004).

Epigenetic events, gene expression alterations that do not alter nucleotide sequences like DNA methylation and histones modification, occur in all stadiums of tumor formation, including premature phases. Due to the genetic alterations caused by these events, they have been recognized as the main mechanisms involved in aberrant silencing of genes, that are important to avoid the initiation and progression of tumors (Ponder 2001). The huge importance of these epigenetic variations is due to the fact that they can be reverted, by applying small molecules like inhibitors of DNA methylation (5-azadeoxycytidine) and inhibitors of histone deacetylase (Moradei *et al.,* 2005; Ting *et al.,* 2006; Momparler, 2003).

Genetic variations acting either inside or outside the cancer cell may determine the outcome of interaction with exogenous carcinogens (Ponder 2001). For instance, sun exposure in individuals with fair skin, chemical exposures and genetic variations in the metabolic pathways may account for substantial differences in cancer susceptibility within the population (Ponder 2001). Moreover, gene-environment interaction may also provide new sights for cancer prevention, since it is possible to categorize subpopulations in terms of genetic risk. This will increase the effectiveness to detect cancers environment causative exposures. This type of information may also be helpful for epidemiologic studies in a way to categorize populations and thus be able to detect the main causes of cancer disease (Ponder 2001). Variations in the circulating levels of hormones or growth factors are also associated with cancer development. For example, high levels of oestrogen might have carcinogenic effects, either through direct stimulation of cancer growth or as a product of mutagenic metabolites (Ponder 2001). Paracrine interactions between inflammatory cells and healthy ones, may also have an important role in cancer development (Ponder 2001). For example, the production of the matrix metalloproteinase 9 by inflammatory cells, has been implicated in the development of squamous cell carcinomas in an HPV-16 transgenic model (Ponder 2001).

1.1.2. Cancer Treatments

A single cancer cell enclosed by healthy tissue will replicate at a higher rate than the normal ones, placing a strain on the supply of nutrients and removal of metabolic wastes. Often tumor cells undergo apoptosis in environments with low nutrients concentrations (such as oxygen, glucose and amino acids) (Nie *et al.,* 2007; Pathak *et al.,* 2007).

Current diagnostic do not reflect the whole clinical heterogeneity of tumors and are insufficient to make predictions for the successful treatment of the disease and patient outcome (Nie *et al.,* 2007). Cancer is often diagnosed in an advanced stage, when cancer cells have already been metastasized and invaded other parts of the body, leading to a loss of effectiveness of the different therapies (Nie *et al.,* 2007).

The usual cancer treatments are limited to chemotherapy, radiation and surgery (Dong and Mumper 2010; Cho *et al.,* 2008). The most recurrent and most active first line of

chemotherapeutic agents are *anthracyclines* (such as doxorubicin, epirubicin and daunorubicin), and *taxanes* (like docetaxel and paclitaxel) (Dong and Mumper 2010).

One of the drawbacks of the existent cancer therapies include nonspecific systemic distribution of the antitumor agents, which leads to body toxicity. The majority of drugs available lack of selectivity for cancer cells resulting in healthy cells death (Brewer *et al.,* 2011; Dong and Mumper 2010; Nie *et al.,* 2007; Peer *et al.,* 2007; Cho *et al.,* 2008). Moreover, the rapid clearance of the therapeutic molecules from blood circulation requires larger doses for the treatment to be effective. Such doses can be responsible for side effects (Brewer *et al.,* 2011; Nie *et al.,* 2007; Peer *et al.,* 2007; Cho *et al.,* 2008). Others obstacles of the current therapies are the inadequate drug concentrations reaching the tumor and the limited ability to monitor therapeutic efficiency (Cho *et al.,* 2008).The biological properties of the solid tumor, that limit drug arrival into neoplasic cells, include abnormal heterogeneous tumor vasculature, interstitium, interstitial fluid pressure and cell density (Dong and Mumper 2010; Peer *et al.,* 2007).

Drug resistance is the major obstacle that limits the therapeutic efficacy of chemotherapeutic agents. Multidrug resistance (MDR) is the phenomenon in which exposure of tumor cells to a single cytotoxic agent accounts for cross-resistance to other structurally unrelated classes of cytotoxic agents (Dong and Mumper, 2010). This is related to the broad spectrum resistance of cancer cells to chemotherapy (Dong and Mumper, 2010). MDR can be caused either by non-cellular mechanisms such as physiological barriers or by cellular ones, like modifications in the biological and biochemical features of the cancer cells (Davis *et al.,* 2008). Non cellular drug resistance may include poorly vascularized tumor regions, high interstitial pressure and low microvascular pressure (Davis 2008). These features appear to significantly reduce drug access to tumor region (Dong and Mumper 2010; Cho *et al.,* 2008; Davis *et al.,* 2008). On the other hand, cellular mechanisms involve changes in specific enzyme systems for drug metabolism, mutations in the drug delivery target and increased drug efflux from tumor cells (Davis *et al.,* 2008). The most widely investigated mechanism of MDR is the change in the membrane transporters that act as drug efflux pumps (Davis *et al.,* 2008). MDR transporters actively pump chemotherapeutic drugs out of the cell reducing intracellular doses to nontherapeutic levels. Not every cancer cell express this type of transporters and chemotherapy drugs are only able to kill cells that do not express MDR transporters or present only a residual expression of these membrane transporters (Peer *et al.,* 2007). One of the most described membrane transporters is glycoprotein P(P-gp), a member of the ABC superfamily (transmembrane proteins that use the energy of ATP hydrolysis to shuttle various substrates across the cell membrane), that is overexpressed in the plasma membrane of tumor cells (Dong and Mumper 2010; Nie *et al.,* 2007; Davis 2008). This glycoprotein is capable of effluxing several anticancer drugs like doxorubicin and paclitaxel out of the cells (Dong and Mumper 2010; Nie *et al.,* 2007). To overcome this problem different inhibitors for this P-gp have been investigated. However, some inhibitors used do not only block the P-gp of tumor cells, but also those from healthy cells, and thus

contributes for the increase of toxicity (causing side effects in different tissues such as bone marrow suppression, cardiomyopathy and neurotoxicity). This limits the drug concentration that reaches the target tissue (Dong and Mumper 2010; Nie *et al.*, 2007).

Enhanced targeting selectivity and delivery efficiency are two of the foremost goals in the development of therapeutic agents. Ideally, a therapeutic drug would be selectively enriched in the tumor with minimal damage to the surrounding healthy tissues, and would have no degradation before reaching the target cells (Dong and Mumper 2010; Cho *et al.*, 2008). In order to overcome both non-cellular and cellular mechanisms of resistance, and to increase drugs selectively towards cancer cells, nanosized devices are currently being developed (Brigger *et al.*, 2002).

1.2. Nanotechnology

Nanotechnology is a multidisciplinary area of research in life sciences, engineering and medicine with broad band applications for molecular imaging, molecular diagnosis and targeted therapy (Misra *et al.*, 2010). The American Nanotechnology Institute defines nanotechnology as a science in which 10−100 nm size structures are developed (Nair *et al.*, 2010; Liu *et al.*, 2007; Farokhzad and Langer 2009). Overtime, the scope of this definition was expanded in terms of its upper limit (Davis *et al.*, 2008), since nanodevices must be large enough to prevent their fast escape into blood capillaries, but small enough to escape from the capture from macrophages, which are lodge in the reticuloendothelial system, like the liver and the spleen. Considering this, the size of the sinusoids in the spleen and fenestra of the Kupffer cells, which varies between 150 to 200 nm, and the size of gap junction between endothelial cells of the leaky tumor vasculature ranges from 100 to 600 nm, nanoparticles size should be at least 100 nm in order to achieve tumour tissues (Cho *et al.*,, 2008). However, due to sieving coefficients measurements for the glomerular capillary wall, and based on the threshold for the first-pass elimination by the kidneys, the lower limit of 10 nm was maintained (Davis 2008).

Nanometer scale devices are mainly built up from their basic constituents since they can be formed by chemical synthesis, spontaneous self-assembly of molecular clusters (molecular self-assembly), biological molecules (e.g., DNA) used as building blocks for production of three-dimensional nanostructures, and quantum dots (nanocrystals) of arbitrary diameter (about 10–10^5 atoms) (Bhushan 2010). Delivery vehicles at nano or micro scale consisting on aggregates of macromolecules have been designed to release the drugs via local injection or systemic release (Baldwin and Kiick, 2010). Methods of imparting biological activity to materials involve the use of polysaccharides derived from natural or synthetic sources. These materials present low immunogenicity, ionic charge and other properties that are fundamental for their use in biomedical applications (Baldwin and Kiick 2010).

1.2.1. Nanoparticles as anti-cancer agents

Nanoparticles were produced 39 years ago as vaccine carriers and chemotherapeutic agents for cancer (Pathak *et al.,* 2007). Cancer nanotherapies have been implemented to undertake several limitations of the conventional drug delivery systems, which are: nonspecific for distribution and targeting, low water solubility, poor oral bioavailability and lower therapeutic efficacy (Yih and Al Fandi 2006).

In contrast to normal cells, tumor anatomical defectiveness along with functional abnormalities such as tumor blood vessels with irregular shape, dilated, leaky or defective and endothelial cells disorganized with large fenestrations, results in extensive leakage of blood plasma components into the tumor. These features help the retention of nanoparticles in tumor site, long enough, to allow local nanoparticle disintegration and release of the drug into tumor's vicinity (Wang and Thanou 2010; Iyer *et al.,* 2006; Liu *et al.,* 2007). Venous return to tumor tissue is slow, lymphatic clearance is poor, but the extravasation into the tumour interstitium continues, leading to an accumulation of macromolecules in the tumor (Iyer *et al.,* 2006). Nanoparticles can penetrate into leaky and hyperpermeable tumor vasculature, accumulate in its proximity using the enhanced permeability and retention effect (EPR). They can also deliver more than one therapeutic agent for combinatory therapy (Danhier *et al.,* 2010; Jain and Stylianopoulos, 2010). This type of approach is currently denominated by passive targeting (figure 4) (Danhier *et al.,* 2010; Cho *et al.,* 2008). However, EPR is not applicable to low molecular weight drugs due to their quick diffusion into the circulating blood, followed by renal elimination (Iyer *et al.,* 2006).

On the other hand, active targeting overcome permeability limitations of the passive targeting since it allows tissue penetration and cellular uptake by cancer cells (Pathak *et al.,* 2007; Peer *et al.,* 2007; Cho *et al.,* 2008). This active targeting involves the functionalization of a carrier system containing the chemotherapeutical agents, which are selectively recognized by the overexpressed receptors existing at the surface of the interest cancer cells, a feature also represented in figure 4 (Pathak *et al.,* 2007; Peer *et al.,* 2007; Cho *et al.,* 2008). Since ligand-receptor interactions can be highly selective, the functionalization of the nanoparticle surface will allow a more precise targeting for tissues of interest and will reduce of the toxic effects in the surrounding normal tissues (Pathak *et al.,* 2007; Peer *et al.,* 2007; Cho *et al.,* 2008). As a result, the potential benefits of such delivery vehicles include: controlled and long-term release rates, extended bioactivity, reduced side effects, decreased administrated frequency to the patient, and the ability to co-deliver multiple drugs with synergistic effects to the same target site (Brewer *et al.,* 2011; Pathak *et al.,* 2007; Farokhzad and Langer 2009).

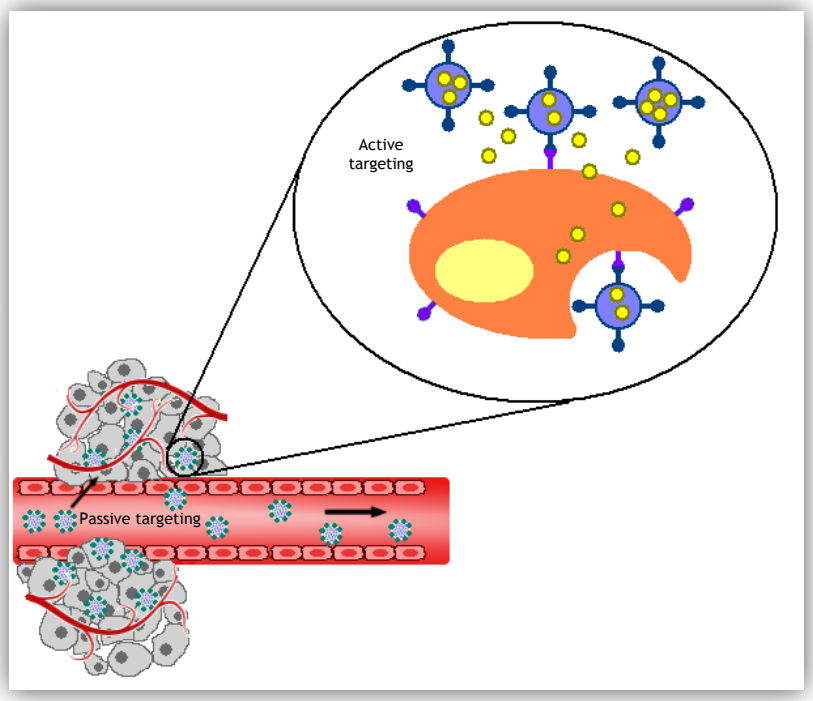

Figure 4 – Schematic representation of different mechanisms by which nanocarriers can deliver drugs into tumors. In the passive mode, nanoparticles accumulate preferential at the tumors sites through EPR , as in the active targeting, ligand molecules such as antibodies and peptides are often used to recognize specific tumor antigens (Adapted from Dong and Mumper 2010; Nie *et al.*, 2010; Farokhzad and Langer 2009)

1.2.2. Nanoparticle surface constituents for a target delivery

The biophysico-chemical features of the carrier such as size, charge and surface hydrophilicity, can all affect both circulating time of the particles and their biodistribution (Farokhzad and Langer 2009). Structures such as antibodies, antibody fragments, small molecules, aptamers (nucleic acids) and peptides, vitamins and carbohydrates have all demonstrated abilities to induce nanoparticle-targeting to cancer cells (Peer *et al.*, 2007).

1.2.2.1 Polymers for nanoparticles' coating

Nanoparticles present a high surface-to-volume ratio when compared with larger particles (Davis, 2008). As a result, the control of nanoparticles surface characteristics is crucial for their administration into human body (Davis, 2008).

The outcome of nanoparticles within the human body can be determined by nanoparticles interactions with their local environment, which depends on a combination of size and surface features (Davis, 2008). Nanocarriers sterically stabilized by polymers like poly(ethylene glycol) (PEG), and with surface charges either slightly negative or slightly positive tend to have minimal self-interactions (Davis, 2008).

The coating of hydrophobic nanoparticles with hydrophilic polymers include common strategies like ligand exchange, micelle encapsulation and covalent bonding (Fang *et al.*,

2009). Synthetic polymers used for coating biomaterials include hydrophilic and non-hydro degradable materials like PEG, poly(vinyl alcohol) (PVA) currently used for coating nanoparticles for oral chemotherapy (Win and Feng 2005), and poly(acrylamide) (PAAm) usually used for coating magnetic nanoparticles (Sun *et al.,* 2006). On the other hand, hydrophobic and hydro degradable polymers are used as well. These include poly(α-esters) good for coating drug delivery systems (Chan-Seng *et al.,* 2009), amphiphilic block polymers like PEG-*b*-PPO-*b*-PEG and thermally sensitive polymers such as poly(N-isopropylacrylamide) (pNIPAAM) that have been used for cancer targeting in conjugation with hyperthermia (Baldwin and Kiick, 2010; Win and Feng 2005).

PEG has been used by different researches as an effective coating material for nanoparticles, due to its ability to resist protein fouling and provide steric hindrance, preventing nanoparticles to aggregate (Fang *et al.,* 2009). PEG is a neutral, crystalline, thermoplastic polymer with a high solubility in water and organic solvents. PEG layers have been added to nanoparticles (liposome, dendrimer or inorganic nanoparticles) that are aimed to be administered intravenously in order to accumulate into tumors (Allen *et al.,* 2002). This approach has been widely applied to form 'stealth' micelles in order to enhance circulation time, by preventing their interaction with plasma proteins, and inhibit the accumulation of opsonises and their uptake by macrophages (Brewer *et al.,* 2011; Dong and Mumper, 2010; Wang and Thanou, 2010). It has been reported that PEG's size and density are the key features that control the circulation times and accumulation in tumors (Dong and Mumper 2010; Wang and Thanou, 2010). PEG is placed on the outmost exterior of the nanoparticle delivery system and targeting ligands are generally presented on top of its layer (Brewer *et al.,* 2010). The enlarged residence time increases the probability of interaction between the receptor and the target cancer cells (Brewer *et al.,* 2011). Akyyama and collaborators studied the effects of PEG grafting level and injection dose on gold nanorod biodistribution in the tumor-bearing mice (Akiyama *et al.,* 2009). This investigation reported that as PEG concentration increases, the amount of gold retained in the spleen decreases, in contrast to the concentrations within the liver and cancer cells (Akiyamai *et al.,* 2009). However, for PEG: gold molar ratios of 1.5 or above, this concentration was higher within the tumor tissue (Akiyama *et al.,* 2009). A decrease in splenic accumulation by increasing the amounts of PEG grafted onto gold nanorods surface can be explained by the ability that particles, larger than 200 nm, have to avoid the reticuloendothelial system and to escape from splenic physical filtration (Akiyama *et al.,* 2009). Gold nanorods that escaped from the spleen were able to reach the tumor tissue and enter within it due to its EPR effect (Akiyamai *et al.,* 2009). Nevertheless, a large amount of PEG may also lead to hepatic accumulation due to the uptake by hepatic parenchyma (Akiyama *et al.,* 2009). This undesired hepatic accumulation of PEGylated nanoparticles might result in an inflammatory response triggered by the liver as described by Cho and colleagues (Cho *et al.,,* 2009).

1.2.2.2. Extracellular matrix targeting ligands for coating nanoparticles

As cancer cells often present similar characteristics to its surrounding healthy tissue, ligands can be designed in order to promote the specific recognition of cancer cells. These molecules have specificity to bind receptors that are overexpressed on cancerous cells. In healthy cells, these nanoparticles should not present capability to induce receptor mediated endocytosis (Brewer *et al.,* 2011). An important aspect is the type of ligand–receptor interaction which modifies the rate of cellular internalization. This rate can affect the accumulation of nanoparticle inside tumor cells (Brewer *et al.,* 2011).

Extracellular matrix (EMC) is mainly composed of proteoglycans and proteins such as collagen, laminin, fibronectin and integrins (Choi *et al.,* 2010). EMC derived short peptides act as receptors binding motifs that can be immobilized or incorporated onto several surfaces, including polymers, hydrogels and nanodevices (Choi *et al.,* 2010).

Sarfati and collaborators performed an investigation that aimed to studied nanoparticles' targeting to lung metastasizes via interactions with the laminin receptor, whose expression is upregulated in metastatic cells (Sarfati *et al.,* 2011). The laminin receptor binding peptide Tyr-Ile-Gly-Ser-Arg (YIGSR) was attached to nanoparticles surface (YIGSR-NPs) to facilitate targeting (Sarfati *et al.,* 2011). When intravenously administered into B16 melanoma tumor – bearing mice, YIGSR-NPs reached the cancerous metastatic cells in lungs, with nearly no binding to the healthy lung cells, which lead to the conclusion that YIGSR-targeted nanoparticles have a potential to be used for systemic delivery of chemotherapeutic drugs for the treatment of metastatic lung cancer (Sarfati *et al.,* 2011) .

Peptides containing the Arg-Gly-Asp (RGD) can be recognized by αß integrins which are overexpressed in tumor cells (Sugahara *et al.,* 2009). RGD sequences have been widely attached to nanoparticles in order to enhance their penetration into tumor vasculature (Sugahara *et al.,* 2009). Kang's group described the ability of gold nanoparticles conjugated with RGD sequence to be recognized by cancer cells (Kang *et al.,* 2010).

Besides integrin receptors, the adhesive glycoprotein fibronectin also appears to play important roles in the progression of cancer disease (Akiyama *et al.,* 1995). Pro-His-Ser-Arg-Asn (PHSNR), the peptide fragment of fibronectin that is recognized by α5β1 receptor of cancer cells, is known for its ability to enhance drug entrapment (KoKKoli 2011). Demirgo and collaborators proposed the incorporation of a fibronectin-mimic peptide into PEGylated lipossomes with the aim of targeting α5β1 which is overexpressed on prostate cancer cells (Demirgo *et al.,* 2008).

There is also a need to optimize ligand density at the drug delivery vehicle surface. Targeting ligands are generally presented on the top of the stealth layer which is attached to the nanoparticles (Wang and Thanou, 2010). This is responsible for the tissue penetration and cellular uptake of the drug delivery systems in order to enhance therapeutic efficacy (Wang and Thanou, 2010; Farokhzad and Langer 2009).

1.2.2.3. Other molecules used for nanoparticles targeting

Antibodies are a group of serum proteins produced by plasma cells that bind specifically to antigens. Regarding targeting, they can be either used in their native state or only as a fragment (Woof and Burton 2004; Peer *et al.,* 2007). Targeting cancer with monoclonal antibodies (mAb) was first described in 1981 (Warenius *et al.,* 1981; Woof and Burton 2004; Peer *et al.,* 2007). Since then, different studies reported their use. In 1997 mAb Rituximab (Rituxan), which binds to antigen CD-20, was approved for the treatment of non-Hodgkin's lymphoma, a cancer originating from lymphocytes. In 1998 Trastuzumud (Herceptin) was approved for breast cancer therapy, binding to human epidermal growth factor Receptor 2 (HER-2) (Peer *et al.,* 2007). Six years later, Bevacizumad (Avastin), an anti-vascular endothelial growth factor (VEGF) mAb, was developed in order to inhibit the factor responsible for the growth of new blood vessels. This antibody was approved for treating colorectal cancer (Peer *et al.,* 2007). Table 1 shows the antibodies and molecules approved by the Food and Drug Administration (FDA) that are often conjugate with nanoparticles to be used in cancer therapy (Cherukuri *et al.,* 2010).

Tabela 1 FDA approved antibodies and molecules currently being used for tumor treatment (Adapted from Adams 2004; Cherukuri, 2010; Ciardiello *et al.,*, 2000; Clemons, 2002; Takimoto and Awada, 2008)

Name	Brand Name	Type	Target	Cancer Type
Bevacizumab	Avastin	Antibody	VEGF receptor	Colorectal, non-small cell, lung, breast
Bortezomib	Velcade	Multicatalytic enzyme	Protein complex proteasome 26 s	Myeloma, lymphoma
Trastuzumab	Herceptin	Antibody	Human epidermal receptor-2 (HER-2)	Breast
Gefitinib	Iressa	Quinazoline derivate; Tyrosine kinase inhibitor	Epithelial growth factor receptor (EGFR)	Non-small cell lung
Sorafenib	Nexavar	Multi kinase inhibitor	Vascular endothelial growth factor receptor (VEGFR) and Platelet derived growth factor receptor	Kidney, liver
Tositumomab	Bexxar	Antibody	Antigen CD20	Lymphoma
Tamoxifen	Nolvadex	Selective estrogen receptor modulator	Estrogen receptor	Breast
Rituximab	Rituxan	Antibody	Antigen CD20	Lumphoma

All antibody molecules possess a similar basic structure comprised of two identical heavy chains as well as two identical light chains. Such chains are arranged to form two antigen binding portions (Fab portion) and one portion that binds to other elements of the immune system like macrophages or other complement proteins (Fc portion) (Woof and

Burton 2004; Peer *et al.,* 2007). In order to have a higher binding activity it is suitable to use the intact antibody. In addition, the binding of immune cells to the Fc portion of de mAb will start a cascade of processes in order to kill the cancer cells. Yet, this mAb portion can also react with the Fc receptors of healthy cells, initiating the immunogenic process (Peer *et al.,* 2007).

In order to increase antibodies efficacy it is possible to conjugate them directly with therapeutic drugs for targeting delivery. However these therapies appear to have some lethal side effects due to nonspecific binding between the targeting agent and non-target receptors on the cell surface (Peer *et al.,* 2007).

The creation of new technologies like fusion proteins (combination of two or more genes producing a new protein with the desired properties) and engineering proteins that are detected by a specific conformation of a target receptor, may improve targeting and selectivity of the drug delivery systems (Peer *et al.,* 2007). Small protein domains like affibodies, a new class of targeting molecules are engineered to bind specifically to different target proteins in a conformational-sensitive manner (Peer *et al.,* 2007). Other small proteins, avimers are used to bind selectively to target receptors through multivalent domains. Heavy-chain antibodies engineered to one tenth of the size of an intact antibody (nanobodies) have been used to bind to carcinoembryonic antigen (CEA), a protein used as a tumor marker (Peer *et al.,* 2007).

Growth factor or vitamin interactions are also used in the targeting strategy, as cancer cells often overexpress the receptors for nutrients to maintain their fast-growing metabolism (Peer *et al.,* 2007). EGFR is overexpressed in a variety of tumor cells such as tongue cancer, epidermal growth factor (EGF) has been shown to block and reduce tumor expression of this receptor (Peer *et al.,* 2007). Folic acid (folate) has also been used in cancer therapy, since folate receptors (FRs) are quite overexpressed in tumors like ovarian, endometrial as well as kidney cancer (Peer *et al.,* 2007). Another example is transferrin (Tf), that interacts with Tf receptors (TFrS), receptors overexpressed in different types of tumors, such as pancreatic, colon, lung, and bladder cancer (Peer *et al.,* 2007). Direct coupling of these targeting agents to nanoparticles containing chemotherapies agents has improved intracellular delivery and therapeutic outcome in animal tumor models (Peer *et al.,* 2007).

Nanomedicine efficacy can be slightly improved by producing nanoparticles that respond to chemical or physical features in the tumor microenvironment (Brewer *et al.,* 2011; Jain and Stylianopoulos, 2010). For instance, nanomaterials can take advantage of cancers lower pH, in order to promote drug delivery (Brewer *et al.,* 2011; Jain and Stylianopoulos, 2010). Hyperthermia is another feature that has been widely investigated as a method for trigger drug release (Brewer *et al.,* 2011). The heat increases microvessel permeability in tumors, which causes the accumulation of the respective thermosensitive nanocarrier in the tumor site, where they release their encapsulated drugs (Brewer *et al.,* 2010). Moreover, hyperthermia also increases cell permeability which induces drug diffusion through tumor walls and sensitivity to thermal injury (Brewer *et al.,* 2011). Nanoparticles can also be design

in order to be activated by the proteinases in tumors (Jain and Stylianopoulos, 2010). In addition, the targeting of nanoparticles to tumors can also be achieved through the use of external sources like magnetic or electric fields, ultrasound and light (Jain and Stylianopoulos, 2010).

By exploiting the varied chemistry of the nanocarriers it is possible to conjugate ligands, polymers and imaging contrast agents all in one type of nanoparticle, as well as make it suitable to accommodate multiple drugs (Park *et al.,* 2009). This multifunctional nanoparticle type is illustrated in figure 5, and is a great promise for the field of individualized medicine (Park *et al.,* 2009).

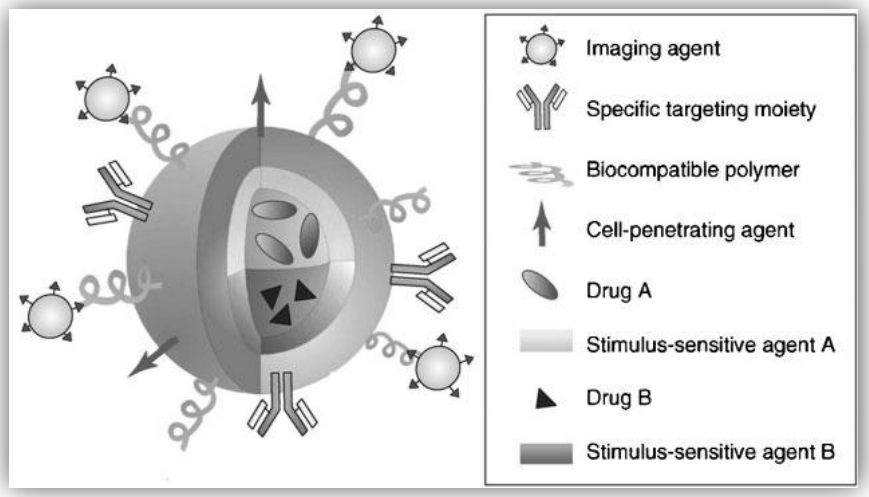

Figure 5 - Illustration of a multifunctional nanoparticle. Multifunctional nanoparticle can combine a specific targeting agent (usually with an antibody or peptide), a cell-penetrating agent, a stimulus-selective element for drug release, a stabilizing polymer to ensure biocompatibility and the therapeutic compound (Adapted from Park *et al.,* 2009)

1.2.3. Different types of nanoparticles

According to the process used to produce nanoparticles it is possible to obtain nanospheres or nanocapsules. Unlike nanospheres (a system in which the drug is dispersed), nanocapsules are vesicular systems in which the drug is confined to an aqueous or oily cavity surrounded by single polymeric membrane. Nanocapsules can then be regarded as a reservoir system (Brigger *et al.,* 2002).

Most of the researchers agree that nanocarriers or nanovectors are nanosized systems that can carry multiple drugs and/or imaging agents. These systems are produced with polymers, ceramics and biological with several shapes, where drugs and contrast agents are attached to. They also possess a corona of polymeric material that improves biokinetics and biodistribution, and a ligand that adds specificity to the particle in order to recognize and attach to cancer cells (Wang and Thanou, 2010; Yih and Al Fandi 2006; Farokhzad and Langer 2009).

The family of nanocarriers includes polymer conjugates, polymeric nanoparticles, lipid-based carriers such as liposomes and micelles, dendrimers, carbon nanotubes, and organic nanoparticles, like ceramic and metallic ones (figure 6) (Peer *et al.*, 2007). These nanocarriers have been explored not only for gene and drug delivery, but also for imaging, photothermal ablation of tumors, radiation sensitizers, detection of apoptosis, and sentinel lymphnode mapping (Peer *et al.*, 2007).

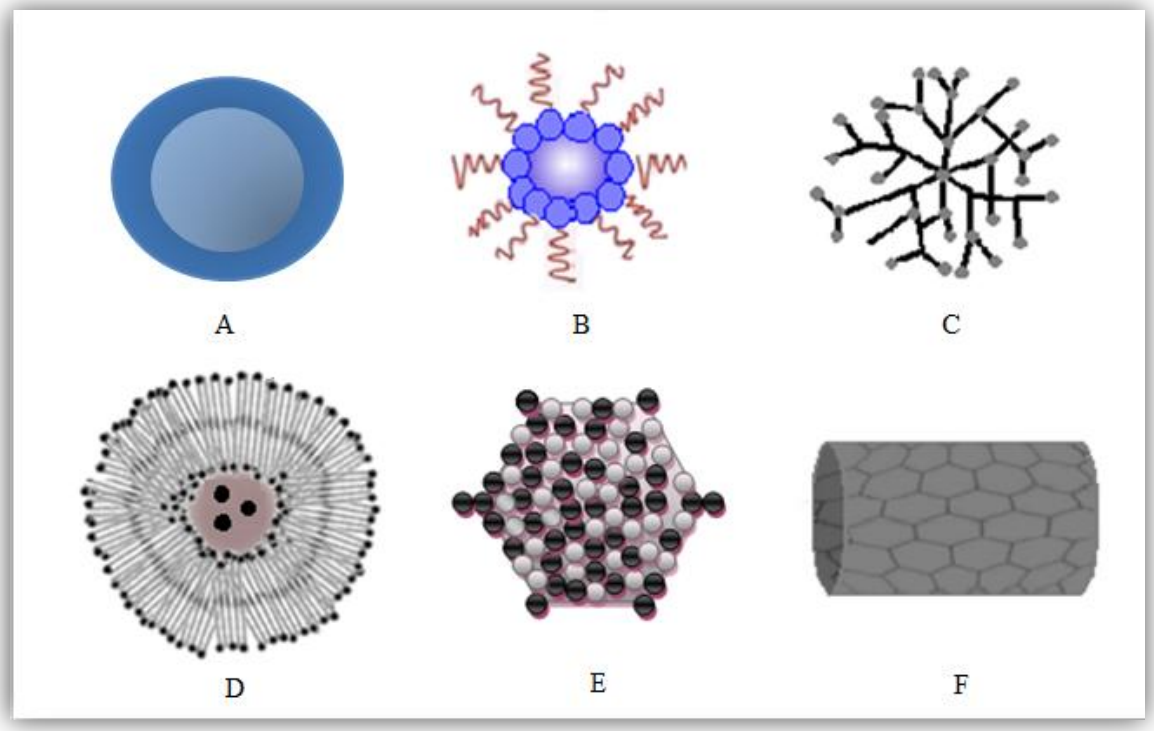

Figure 6 – Different types of nanoparticles for drug delivery: Polymeric nanoparticles (A); polymeric micelles (B); Dendrimers (C); Liposomes (D); Viral-based nanoparticles (E); Carbon nanotubes (F) (Adapted from Cho *et al.*, 2008)

1.2.3.2. Amphiphile-based particles

Amphiphile molecules are made of two different fractions or 'blocks', one hydrophilic and other hydrophobic (Discher and Ahmed 2006). Liposomes, polymersomes, and micelles represent a class of amphiphile-based particles (Wang and Thanou 2010).

1.2.3.2.1. Liposomes

Liposomes are considered the most intensively researched colloidal drug delivery systems (Wang and Thanou 2010). These particles have a size in the nanoscale range and consist of a lipid bilayer surrounding a water core loading the drug. Since they are made of natural materials, liposomes are safe drug carriers that can circulate in the bloodstream for a long period of time (Wang and Thanou 2010). Nowadays, liposomes are approved by regulatory agencies to be used for chemotherapeutics since they can transport anticancer

drugs without affecting normal cells. Liposomes can be loaded during its production with hydrophilic or hydrophobic drugs. However, when adding charged hydrophilic drugs, there is a need to use pH-gradient between the internal and external aqueous domains. This gradient drives the drug into the interior of liposomes by partitioning through the membrane. On the other hand liposomes have poor loading capacity for hydrophobic drugs (Dong and Mumper 2010; Wang and Thanou 2010; Cho *et al.*, 2008). Liposomes were first developed in order to improve the pharmacokinetics and biodistribuition of the drug doxorubicin (Wang and Thanou 2010). This drug appears to induce cardiotoxicity which limit the administered dose. In this perspective, doxorubicin was encapsulated into anionic liposomes leading to an improvement in drug accumulation in tumors and decreasing its side effects. Liposomal doxorubicin has also shown to be efficient and save in the treatment of ovarian and breast cancer (Wang and Thanou 2010). Another approved nanoparticle for cancer therapy was Abraxane (an albumin Taxol) that was produced to overcome Taxol insolubility. Abraxane is an improvement of Cremophor EL that used solvents (polyethoxylated castor oil) to solubilise Taxol (Table 2). Endogenous hydrophobic molecules bound to albumin through non covalent interactions, which makes albumin a natural carrier for this type of molecules (Wang and Thanou 2010). Therapeutic nanocarriers based on this strategy have been improved and approved for a wider use (Peer *et al.*, 2007). Liposomal systems have shown preferential accumulation in tumors via EPR effect and also present reduced toxicity, being therefore very suitable for clinical practice. On the other hand, long-circulating liposomes may lead to extravasation of the drug in unexpected locals (Peer *et al.*, 2007). This can cause palmar-plantar erythrodysesthesia (PPE) also denoted as hand-foot syndrome, a dermatologic toxicity reaction seen when high doses of chemotherapy are used and that can be solved by changing the doses and scheduling of the treatment (Peer *et al.*, 2007). However, liposomes lack controlled release mechanisms and present some limitations like pharmacokinetic shortcomings (Dischер and Ahmed 2006).

Table 2 – Examples of clinical approved tumor target nanoparticles (Adapted from Jain and Stylianopoulos; Davis *et al.*, 2008; Lammers *et al.*, 2008)

Compound	Name	Cancer Indication
Liposomal doxorubicin	Myocet,Caelyx(Doxil)	Breast, Ovarian
Liposomal daunorubicin	Daunoxome	Kaposi Sarcoma
Liposoaml vincristine	Onco- TCS	Non-Hodgkin Lymphoma
Albumin-paclitaxel	Abraxane	Breast
90Yttrium- Ibritumomab tiuxetan (α-CD20)	Zevalin	Non-Hodgkin Lymphoma
DTA- IL2 fusion protein (α-CD25)	Ontak	T-cell Lymphoma
Ozogamycin-gemtuzumab (α-CD25)	Mylotarg	Leukemia

1.2.3.2.2. Polymersomes

Polymersomes are self-assembled shells composed of a block copolymers amphiphiles that have been widely engineered to perform some of the functions as viral capsids (Ahmed *et al.,* 2006; Discher and Ahmed 2006; Meng *et al.,* 2009). This type of particles have also shown remarkable applications in medicine and biotechnology, since they are able of transporting hydrophilic as well as hydrophobic species such as anticancer drugs, genes, proteins and diagnostic probes (Ahmed *et al.,* 2006; Discher and Ahmed 2006; Meng *et al.,* 2009).

Unlike liposomes, polymersomes are in general prepared from macromolecular amphiphiles of various architectures including amphiphilic blocks, graft and dendritic copolymers (Ahmed *et al.,* 2006; Discher and Ahmed 2006; Meng *et al.,* 2009). Incorporation of biomolecules as well as a broad spectrum of functionality suggests that these synthetic carrier systems offer a truly generic approach for drug delivery (Meng *et al.,* 2009).

1.2.3.2.3. Micelles

Micelles are self-assembling lipid monolayers with a hydrophobic core and hydrophilic shell, that have been used with success in the transport of water-insoluble drugs (Phillips *et al.,* 2010; Peer *et al.,* 2007). As liposomes, micelles belong to the group of amphiphilic colloids that can be formed spontaneously under certain concentrations and temperatures from amphiphilic or surface-active agents (Peer *et al.,* 2007).

Polymeric micelles are non-biodegradable, stable in biological environments and, due to its small size (<100nm) and flexibility to incorporate the drug, can effectively reach the solid tumors since they are able to take advantage of the EPR effect of cancer cells(Dong and Mumper 2010; Cho *et al.,* 2008).

1.2.3.3. Dendrimers

Dendrimers are the main polymeric architectures that are constructed from a series of branches around a core, providing products of different generations with a nearly perfect 3D geometry pattern (Wang and Thanou 2010). Dendrimers are versatile particles, with special features like size, functionality and chemistry, that makes them good candidates for several modifications in certain imaging modalities (Wang and Thanou 2010). They are more expensive than other nanoparticles and require many repetitive steps for synthesis, which is a challenge for large-scale production (Peer *et al.,* 2007). This type of nanodevices can be synthesized with either divergent methods (outward from the core) or convergent ones (inwards towards the core) (Peer *et al.,* 2007). An example of this type of nanocarries is Polyamidoamine (PAMAM) synthesis using divergent methods. This agent can be easily conjugated with targeting molecules, imaging agents and drugs, since they present high water

solubility and well defined chemical structures, are biocompatible, and present good clearance due to their small size (<5nm) excluding the need of biodegradability (Wang and Thanou 2010).

Dendrimer-methotrexate conjugates are used in *in vivo as* drug delivery systems resulting in a tenfold reduction in tumor size compared with that achieved with the same molar concentration of free systemic methotrexate (Peer *et al.,* 2007).

This type of nanodevices can either carry drugs as complexes or as conjugates. However, controlling the rate of drug release from dendrimer is a difficult assignment since encapsulated drugs tend to be released before reaching the target site. The conjugated ones have their release controlled by the chemical linkage between the dendrimer and the drug (Dong and Mumper 2010; Phillips *et al.,* 2010; Wang and Thanou 2010; Peer *et al.,* 2007; Haley and Frenkel 2008).

Gadolinium has also been complexed with dendrimers in order to improve conventional magnetic resonance (MR) images and it has shown better images then that obtained with the usual diethylenetriaminepentaacetic acid Gd (III) chelate (Wang and Thanou 2010).

1.2.3.4. Carbon nanotubes

Carbon nanotubes are extremely small tubes with one or more carbon sheets (Wang and Thanou 2010; Peer *et al.,* 2007). They are completely insoluble in all solvents which may lead to some toxicity. To solve this, carbon nanotubes can be chemically modified in order to make them water soluble and be able to be conjugated with a wide variety of active molecules such as peptides, proteins, nucleic acids and therapeutic agents, like doxorubicin and paclitaxel. Carbon nanotubes have been applied in biology as sensors for detecting DNA and proteins, diagnostic devices for the discrimination of different proteins from serum samples, and carriers to deliver vaccines or proteins (Wang and Thanou 2010; Peer *et al.,* 2007). The multiple covalent functionalizations on the sidewall or tips of carbon nanotubes allows them to carry several molecules at once which is advantageous for cancer therapy (Cho *et al.,* 2008).

Several studies have been made in order to understand the type of blood stream circulation of carbon nanotubes and if they do accumulate in target tissues or cells. Drugs conjugated with this nanodevice have been shown a more effective internalization into cells when compared to the free drug alone (Cho *et al.,* 2008). Some studies concerning carbon nanotubes have also demonstrated the existence of a high antifungal activity (Cho *et al.,* 2008).

1.2.3.5. Inorganic nanoparticles

Inorganic nanoparticles are mainly metal based and have been widely investigated for MRI as well as high-resolution superconducting quantum interference devices (Peer *et al.,* 2007; Rotello 2008). The inorganic component of the particles imparts exceptional features to the resultant systems, providing capabilities for both delivery and imaging applications (Peer *et al.,* 2007; Rotello 2008). Since inorganic nanoparticles are usually smaller and do not present the flexibility of polymeric nanoparticles and liposomes, the conjugation between inorganic ones and polymers is suitable in order to enhance nanoparticles blood circulation time as well as tissues targeted uptake (Wang and Thanou, 2010). Some examples of inorganic nanoparticles are briefly described below.

1.2.3.5.1. Ceramic nanoparticles

Ceramic nanoparticles are one example of nanoparticles produced with inorganic materials and are known for their porous structure that can be easily produced with a desired size and porosity. These features have great interest to its use as drug vehicles (Wang and Thanou, 2010). Some of the ceramic nanoparticles used in cancer therapy are produced with alumina, silica and titania (Zhang *et al.,* 2007). These nanoparticles possess high physiological stability and can be loaded with DNA to destroy, for instance, cancerous liver cells (Yih and Al Fandi 2006). Hydroxyapatite nanoparticles have been used for insulin release, presenting promising results regarding to repeated injections (Yih and Al Fandi 2006).

1.2.3.5.2. Metallic nanoparticles

Another type of inorganic nanoparticles are those produced with metallic ions. They can be synthesized with small sizes (<50nm) but their high surface area allows them to transport high doses of drugs. Metallic nanoparticles can also release the drug to the target site using for this purpose a source of external excitation, such as infrared light or a magnetic field (Gunasekera *et al.,* 2009). Specific types of recently developed inorganic nanoparticles include iron oxide nanoparticles, nanoshells and gold nanoparticles (Wang and Thanou 2010; Peer *et al.,* 2007). As mentioned above, magnetic nanoparticles composed of a magnetic core and biocompatible polymeric shell have been widely used in tumor target delivery and magnetic resonance imaging (MRI) (Chertok *et al.,* 2008; Sun *et al.,* 2008). Iron oxide magnetic nanoparticles are known to be strong enhancers of proton spin–spin relaxation, which makes them suitable for a noninvasive detection of MRI signal (Chertok *et al.,* 2008). Due to the reduction in signal intensity (negative contrast) at the spatial location of magnetic nanoparticles it is possible to visualize them at the MRI images collected under *in vivo* conditions (Chertok *et al.,* 2008).

Nanoshells with size ranging from 100–200 nm may be used both for imaging and therapy (Wang and Thanou 2010; Peer *et al.,* 2007). They present optical resonances that can be adjusted to absorb or scatter anywhere in the electromagnetic spectrum, including the near infrared region (NIR), where transmission of light through tissue is optimal (Peer *et al.,* 2007). Absorbing nanoshells are suitable for hyperthermia-based therapeutics, where nanoshells absorb radiation and heat up the surrounding cancer tissue, as scattering nanoshells are desirable as contrast agents for imaging applications (Peer *et al.,* 2007).

A similar approach involves the use of gold nanocages, which are smaller (<50 nm) than nanoshells, to generate heat in response to NIR light and thus may also be useful in hyperthermia-based therapeutics (Peer *et al.,* 2007).

1.2.3.5.2.1. Gold nanoparticles

Healthy tissue toxicity caused by non-specific interactions may hold back the use of many types of nanoparticles (Peer *et al.,* 2007). If inorganic particles are used for photo-ablation, they are going to avoid non-specific toxicity, since light is locally directed (Peer, *et al.,* 2007). Gold nanodevices seem to exhibit low toxicity (Huang and El-Sayed 2010; Nelson and Rothberg 2011; Chen *et al.,* 2008). However it is extremely important to take into account that cytotoxicity is strongly dependent on the exact nature of the gold nanoparticles (AuNP's) (Schlehe *et al.,* 2011).

AuNP's are relatively easy to synthesize and manipulate (Peer *et al.,* 2007) and monodisperse nanoparticles can be formed with core sizes ranging from 1 nm to 150 nm, with chemically active surfaces that bind to amine and thiol groups (Nelson and Rothberg 2011; Selvakannan *et al.,* 2003; Ghosh *et al.,* 2008). The most popular technique to produce AuNP's is by the chemical reduction of gold salts using citrate as a reducing agent. This method was used for the first time in 1973 by Frens (Frens 1973; Chen *et al.,* 2008). Very small AuNP's can be misrecognized by cellular barriers as biological compounds, leading to undesired cellular entry which can compromise normal cellular function (Schleh *et al.,* 2011; Chen *et al.,* 2008). These particles can be incorporated into the groves of DNA molecules and thereby induce oxidative stress (Schleh *et al.,* 2011). In 2007, Pan and colleagues demonstrated that AuNP's display a size dependent cytotoxicity with AuNP's with sizes ranging from 1 to 2 nm being considered toxic, and 15 nm AuNP's as nontoxic, confirming the results previously reported in several studies, in which AuNP's presented a size dependent toxicity (Chen *et al.,* 2008). This characteristic can be taken into consideration in order to induce DNA damage and therefore cellular apoptosis of cancer cells. Recent studies report the functionalization of AuNP's with specific sequences like RGD sequences and nuclear localization signal (NLS) peptide in order to improve the delivery of these nanoparticles into cancer cells (Kang *et al.,* 2010).

Another feature that appears to interfere with AuNP's cytoxicity is their surface charge. Nevertheless this particular aspect is still raising some conflicts and as some authors

suggested that both cationic and anionic AuNP's present toxicity (Schaeublin *et al.,* 2011; Murphy *et al.,* 2008), while others indicate that only those presenting cationic side chains have a moderate toxicity (Chen *et al.,* 2008; Murphy *et al.,* 2008). Both the method and the type of surface coating play an important role when trying to understand AuNP's cytotoxicity (Lewinski *et al.,* 2008).

For biomedical applications, surface functionalization of AuNP's is essential to apply them to specific disease areas and allow them to selectively interact with cells or biomolecules (Shenoy *et al.,* 2006). PEG modification of nanoparticles allows them to remain in the systemic circulation for a long period of time (Øie 2004; Shenoy *et al.,* 2006).

As therapeutic delivery agents, AuNP's can be loaded both with small drug molecules like anti-angiogenic and anti-cancer agents and large biomolecules, like proteins, DNA or RNA (Kang, *et al.,* 2010; Wang and Thanou 2010; Chen *et al.,* 2008; Ghosh *et al.,* 2008). Efficient release of these therapeutic agents is a prerequisite for an effective therapy (Ghosh *et al.,* 2008). The release could be triggered by internal stimuli like pH variations (Polizzio *et al.,* 2007; Ghosh *et al.,* 2008), or by external stimulus such as infrared light or a magnetic field (Wang and Thanou 2010; Ghosh *et al.,* 2008).

Also relying on their size, shape, degree of aggregation, and local environment, AuNP's can appear red, blue, or in other colors (Murphy *et al.,* 2008). When a metal particle is exposed to light the electromagnetic field leads to a collective coherent oscillation of the free electrons of the metal, that oscillate around the particles surface causing a charge separation according to the ionic lattice (Huang and El-Sayed, 2010). This electron fluctuation forms a dipole that oscillates according to the direction of the electric field of the light. The amplitude of the oscillation reaches a maximum at a specific frequency called surface plasmon resonance (SPR) (Huang and El-Sayed, 2010). Once excited, the SPR of AuNP's can scatter and/or absorb light both in the visible and the NIR spectrum, which is an exceptional useful property for *in vivo* optical imaging techniques like MRI, X-ray Computed Tomography (X-ray CT), Biosensing and Photothermal Therapy (PTT) (Chen *et al.,* 2008). As for MRI, AuNP's have been widely used as a delivery vehicle to convey multiple gadoliniumdiethyltriamenepentaacetic complexes (the most widely used contrasting agent for MRI) into selective cellular targets (Chen *et al.,* 2008).

X-ray CT is another non-invasive diagnostic tool that often makes use of contrasting agents in order to enhance the contrast between cells. However, the usual agents used for this purpose also present some limitations like renal toxicity, vascular permeation and rapid renal excretion which lead to limited imaging interval (Chen *et al.,* 2008). This limitation appears to be overcome by using AuNP's since this type of nanoparticles present higher X-ray absorption coefficient and a surface that can be easily modified in order to enhance their circulation time in the body (Wang and Thanou, 2010 ; Chen *et al.,* 2008).

This type of metal particles absorb light around the 520nm and almost 100% of the absorbed light is converted to heat via a series of nonradiative processes (Chen *et al.,* 2008). These characteristics as well as photostability and biocompatibility makes AuNP's suitable as

contrast agents for PTT in which photon energy is converted to heat in order to induce cellular events like hyperthermia, coagulation and evaporation (Cherukurir *et al.,* 2010; Huang and El-Sayed 2010; Chen *et al.,* 2008). This type of therapy holds a huge promise for the treatment of cancer and related disease conditions (Huang and El-Sayed 2010; Cheni *et al.,* 2008).

Regardless of particle composition, as soon as particles are injected intravenously, they are rapidly cleared from the bloodstream by reticuloendothelial defense mechanism. Instability of the carrier and burst drug release, as well as non-specific uptake by the mononuclear phagocytic system (MPS) are challenges that need to be overcome in order to apply these carriers into the clinic.

1.3. Oligoaziridine probe for capping nanoparticles

Biosensors have been widely used in several applications like food processing, environmental monitoring and clinical diagnosis. These optical sensors are molecular receptors whose optical properties change upon binding to specific guests (Chen *et al.,* 2008; Valeur and Leray, 2000). One of the main applications of biosensores is in the detection of toxic and carcinogenic metals in environmental samples. Raje and colleagues successfully designed a new fluorescent probe based on the polymerization of aziridines for copper (Cu^{2+}) detection. The investigators reported that when oligoaziridine biosensor was added to human fibroblast cells and a fluorescence emission was observed. After treating the cells with 20 µg/mL of cooper the intracellular fluorescence decreased along time (Raje *et al.,* submitted manuscript)

The decision of working and investigated gold nanoparticles relied in their fantastic features like small size, inert capabilities as well as unique chemical and physic properties (Huang and El-Sayed 2010; Nelson and Rothberg 2011; Selvakannan *et al.,* 2003; Liu *et al.,* 2007; Peer *et al.,* 2007; Shan and Tenhu 2007; Chen, *et al.,* 2008; Ghosh *et al.,* 2008; Murphy *et al.,* 2008). Oligoaziridine is a new optical sensor that can be coupled to nanoparticles in order to evaluate their internalization by cells, in an environment free of Cu^{2+}. Also, capping AuNP's with oligoaziridine makes it possible to track nanoparticles course in the cells, bringing new sights for optimal imaging using gold nanoparticles, when methodologies like X-ray CT and MRI are not recommended or available.

Chapter II -Materials and Methods

2.1. Materials

A549 non-small lung carcinoma cell line was purchased from ATCC (Middlesex, UK). Sodium azide was purchased from Amresco. Fetal bovine serum (FBS) was purchased from Biochrom AG (Berlin, Germany). Tris Base was purchased from Fisher Scientific. Glass bottom dishes (35mm dishes, 10mm glass, 0mm thickness) were purchased by MatTek Corporation (USA). Maleimide-PEG-Maleimide (MAL-PEG-MAL) was purchased from NANOCS. Tetrachloroauric (III) acid ($HAuCl_4.3H_2O$), 3-(4,5-dimethylthiazol-2-yl)-5-(3-carboxymethoxyphenyl)-2-(4-sulfophenyl)-2H-tetrazolium reagent MTS, Trisodium citrate, Triethylamine, Amphotericin B, L-glutamine, Ham's Nutrient Mixture-F12, ethanol (EtOH), glutaraldehyde, penicillin G, phosphate-buffered saline (PBS), streptomycin, trypsin and collagen solution were purchased from Sigma (Sintra, Portugal).

2.2. Methods

2.2.1. Preparation of gold nanoparticles by the citrate reduction method - *Method 1*

The preparation of gold nanoparticles was initiated with the addition of 100 ml 0.01% (w/v) tetra-chloroauric[III] acid trihydrate ($HAuCl_4.3H_2O$) which was heated to boiling under reflux conditions. 1mL of trisodium citrate hydrate 1% (w/v) was added to the boiling solution under constant stirring. After 25s, a slightly yellow solution will turn faintly blue (nucleation). Then, the blue color suddenly changed into dark red, indicating the formation of monodisperse spherical particles. The solution was boiled for another 5m to complete reduction of the gold chloride. The absorbance of such suspensions, measured with Ultrospec 3000 from Pharmacia Biotech at 540nm. The gold nanoparticles obtained were supplemented with 0.05% (w/v) sodium azide in order to be stored at 4°C for several months (Frens 1973). Gold nanoparticles produced by this method will be referred as AuNP's_F.

2.2.2. Production of gold nanoparticles by oligoaziridine reduction assay- *Method 2*

$HAuCl_4.3H_2O$ (10^{-3} M) was reduced by the addition of oligoaziridine, in order to obtain the final biosensor concentrations of 0,372mg/mL; 0,0372mg/mL and 0,00745mg/mL. The reaction was performed under stirring and mild heating (50°C). The gold nanoparticles produced were subjected to ultracentrifugation (using a Hermle Z323K centrifuge), at 14500g, during 20m, at room temperature. The supernatant was removed and the pellet was washed several times with deionized water in order to remove all the non-reactive groups.

Once again, the pellet was resuspended in deionized water in order to be used for the following assays (Aslam *et al.*, 2004). The produced nanoparticles were characterized by Scanning Electron Microscopy (SEM), Ultraviolet–Visible (UV-VIS) spectroscopy, Fourier Transform Infrared (FTIR) spectroscopy, and will be named as OligoNP's.

2.2.3. Coating gold nanoparticles prepared by method 1 with oligoaziridine

Three different concentrations of oligoaziridine were added to the colloidal solution of gold nanoparticles prepared by method 1. Oligoaziridine was added to the colloidal suspension in order to obtain the concentrations previously mentioned in sub-section 2.2.2 and vortexed at low speed, during 2m. The samples were then ultracentrifuged at 14500g, during 20m, at room temperature. The supernatant was then removed and the pellet was redispersed in deionized water for all the subsequent tests. The formed nanoparticles were evaluated by SEM analysis, UV-VIS spectroscopy and FTIR spectroscopy, and will be denoted as Au_Oligo.

2.2.4. Coating gold nanoparticles prepared by method 1 with homofunctional maleimide poly(ethylene glycol)

Gold nanoparticles produced by method 1 were capped with MAL-PEG-MAL (AuNP's_PEG). First, PEG was added to gold nanoparticles in several ratios (PEG: AuNP's) 500:1, 750:1, 1000:1, 2500:1, 5000:1, 10.000:1 (Liu *et al.*, 2007). In order to obtain these molar ratios, there was a need of calculating AuNp's molar concentration.

—— Eq. (1)

where, N_{total} is the total number of gold atoms, N the total number of atoms per nanoparticles, C solution molar concentration (M), V solution volume (L) and N_A Avogadro's number (Liu, Atwater *et al.*, 2007).

The total number of gold atoms, N_A was also calculated according to the following equation:

– — Eq. (2)

with ρ being gold density, D average size of the particles and W the molecular weight (Liu, Atwater *et al.*, 2007).

Therefore, a proportion of PEG to satisfy both molar ratios was added to 10 mL of colloidal gold solution and the reaction was performed during one hour under stirring (Liu, *et al.*, 2007).

Afterward, the mixture was collected to 1,5mL eppendorfs and was centrifuged at 13500g, for 20m at room temperature. The supernatant was removed and the pellet was redispersed in Tris buffer (pH 7.4) and stored at 4°C, until further use.

In order to choose the most suitable PEG:AuNP's ratios, i.e. the most perfect pegylated particles to performed the subsequent in vitro studies, all the nanoparticles produced were carefully analyzed by SEM, UV-VIS spectroscopy, FTIR spectroscopy and X- ray diffraction (XRD).

2.2.5. Coating AuNP's_PEG with oligoaziridine

Oligoaziridine was also added to AuNP's_PEG. For this reaction takes place, the selected samples were once again ultracentrifuged with the same parameters previously described in subsection 2.2.4. The samples were resuspended in water and the three different oligoaziridine concentrations (0,372mg/mL, 0,0372mg/mL and 0,00745mg/mL) were added to the selected AuNp's PEG particles. The mixtures were stirred during 1h in the dark and then re-centrifuged at 13500g, for 20m, at room temperature. The supernatant was removed and the pellet was redispersed in deionize water, for subsequent analyses of SEM images, UV-VIS spectroscopy and FTIR spectroscopy. The nanoparticles produced with this procedure will be designated AuNP's_PEG_Oligo.

2.2.6. Scanning electron microscopy analysis

The morphology of the nanoparticles herein produced was characterized by SEM. All the nanoparticles produced in this work were air-dried overnight and then mounted on an aluminium board using a double-side adhesive tape and covered with gold using an Emitech K550 (London, England) sputter coater. The samples were then analyzed using a Hitachi S-2700 (Tokyo, Japan) scanning electron microscope operated at an accelerating voltage of 20 kV and at various amplifications (Gaspar *et al.*, 2011; Ribeiro *et al.*, 2009)

2.2.7. Ultraviolet –Visible Spectroscopy

UV-VIS spectroscopy is the most widely used methodology to characterize optical and electronic properties of the particles (Philip 2008). This method is based in ultraviolet and visible radiation which is absorbed by the samples.

All UV-VIS spectra were recorder using UV-1700 PharmaSpec from Shimadzu at 300 nm/min scanning rate in a wavelength range from 350 to 750nm, and then analyzed with UVProbe Shimadzu 2.0 software.

2.2.8. Fourier Transform Infrared spectroscopy

In infrared spectroscopy the radiation crosses the sample and some of the radiations are absorbed while others are transmitted. The resulting spectra represent the frequency of vibration between the atoms linkage from the sample, creating therefore, a specific spectra for those interactions (Bacsik *et al.,* 2004). The produced nanoparticles were analyzed and recorded on a Fourier transform infrared spectrophotometer Nicoletis 20 (64 scans, at a range of 4000 to 400cm^{-1}) from Thermo Scientific (Waltham, MA, USA) equipped with a Smart iTR auxiliary module.

2.2.9. X-Ray Diffraction

XRD is a nondestructive technique used to identify and determine crystalline phases and crystal orientation, structural features and atomic arrangement (Nistor 2008; Perera *et al.,* 2010; Kockelmann and Kirfel 2006). In order to proceed to the XRD analysis of the nanoparticles, the samples were lyophilized and then mounted in silica supports using a double sided adhesive tape. The experiments were performed over the range from 5° to 90° 2θ with continuous scans at a rate of 1° 2θ min^{-1}, using a Rigaku Geigger Flex D-max III/c diffractometer (Rigaku Americas Corporation, USA) with a copper ray tube operated at 30kV and 20mA (Gaspar *et al.,* 2011).

2.2.10. Proliferation of A549 non-small lung carcinoma cell line in the presence of the produced nanoparticles

Cell culture experiments were performed with a A549 non-small lung carcinoma cell line cultured in Ham's F12K medium supplemented with 10% v/v heat-inactivated FBS and antimycotic (penincilin G(100 U/mL)), spectromycin G(100µg/mL), at 37°C, under 5% CO_2 humidified atmosphere. Cells were seeded in 25cm^3 T-flasks until confluence be obtain and then, cells were sub cultivated by incubation on 0.18% trypsin (1:250) with 5mM EDTA (Gaspar *et al.,* 2011). Then, cells were centrifuged, resuspended in culture medium and seeded in T-

flasks of 75cm^3. After this, cells were kept in culture at 37ºC, with 5% CO_2 humidified atmosphere (Maia *et al.*, 2009; Ribeiro *et al.*, 2009). In order to evaluate cell behavior in the presence of the nanoparticles herein produced, A549 cells were seeded with the nanodevices in a 96 well plates at a density of 12x10^3 cells/well, for 24h. Before cell seeding, plates and the materials were sterilized by UV exposure for 30m (Ribeiro *et al.*, 2009). Cell growth was monitored using an Olympus CX14 inverted light microscope (Tokyo, Japan) equipped with an Olympus SP-500 UZ digital camera. This last procedure was repeated for 2 days.

2.2.11. *In vitro* transfection of cells with the nanoparticles produced

In vitro transfection studies were carried out by seeding the cells in glass bottom dishes, at a density of 12 x10^{3}cells per well, with 1mL of Ham's F12K medium supplemented with 10% FBS without antibiotic, in order to promote cell transfection. The cells were allowed to growth for 24hours. The transfection of cells with all type particles produced was performed and after 4 hours the transfection process was stopped, by exchanging the medium for complete Ham's F12K medium.

2.2.12. Qualitative Evaluation of *in vitro* transfection

In order to evaluate the ability of nanoparticles to enter within the cells, both immunofluorescence and CLSM assays were performed after the *in vitro* transfection. First, the glass bottom dishes containing transfected live cells were visualized using a Zeiss AX10 microscope and analyzed with Axio Vision Real 4.6 software (Carl Zeiss SMT Inc., USA). Then, CLSM was used to visualize the intracellular localization of the produced nanoparticles in living cells. Confocal and bright field images were obtained with a Zeiss LSM 710 laser scanning confocal microscope (Carl Zeiss., USA) equipped with a plane-apocromat 40x/DIC objective. Data analysis of CLSM images was performed with Zeiss software (Axio Vs40 V4.5).

2.2.13. Evaluation of the cytotoxic profile of the produced nanoparticles

In order to evaluate nanoparticles toxicity, the MTS assay was performed. All nanoparticles herein produced were applied into a 96 well plate (n=5) and irradiated under UV light for 30m before cell seeding. To perform the MTS assay A549 cells were seeded in a 96 well plate containing the biomaterials, at a density of 12x 10^3 cells per well. Then, 100µL of culture medium was added to each well and the plate was incubated at 37 °C, in a 5% CO_2 humidified atmosphere (Ribeiro *et al.*, 2009).

After an incubation of 24 and 48h, the mitochondrial redox activity of the viable cells was assessed through the reduction of the MTS into a water-soluble purple formazan product.

The medium of each well was then removed and replaced with a mixture of 100µL of fresh culture medium and 20µL of MTS/PMS (phenazine methosulfate) reagent solution. The cells were incubated for 4h, at 37°C, under a 5% CO_2 atmosphere. The absorbance was measured at 492nm using a microplate reader (Sanofi, Diagnostics Pauster). Wells containing cells in the culture medium without materials were used as negative control. EtOH 96% was added to wells containing cells as a positive control (Palmeira-de-Oliveira *et al.*, 2010, Ribeiro *et al.*, 2009).

2.2.14. Statistical analysis

Statistical analysis of cell viability results was performed using one-way analysis of variance (ANOVA) with the Dunnet's post hoc test. A value of $p< 0,05$ was considered statistically significant (Ribeiro *et al.*, 2009). The results obtained for cells in the presence of different carriers were compared with the negative and positive controls. Computations were performed using a MYSTAT 12 statistical package (Systat Software, a subsidiary of Cranes Software International Ltd.).

Chapter III - Results and Discussion

3. Results and Discussion

In the following sub-sections it will be described a series of results that were obtained in the different assays and discussed the linkage of oligoaziridine to the produced nanoparticles.

3.1. Particles Morphology

As previously described, SEM images were used to evaluate the morphology of the nanoparticles produced.

In the present study gold nanoparticles were produced by two different methods. The nanoparticles obtained had different sizes. Gold nanoparticles produced by method 1 were prepared according to a study performed by Frens in 1973. This procedure intended to produce nanoparticles with an average size of 40nm. The SEM analysis performed revealed particles with spherical shape and with sizes ranging from 42 to 62nm (Figure 7A).

In order to produce Au_Oligo nanoparticles, 3 different oligoaziridine concentrations were added to the colloidal suspension of particles produced by method 1. SEM images of Au_Oligo_1 (AuNP's_F coated with 0,372mg/mL of oligoaziridine) revealed aggregates not forming, therefore, spherical nanoparticles. The SEM images of Au_Oligo_2 nanoparticles (AuNP's_F coated with 0,0372mg/mL of oligoaziridine) also presented some aggregates dispersed in the solution (however less than those found for Au_Oligo_1 particles). In the case of Au_Oligo_3 nanoparticles (AuNP's_F coated with 0,00745mg/mL of oligoaziridine), the SEM analysis showed nanoparticles with sizes ranging from 154 to 165nm (Figure 7B). No particles aggregation was observed in this case.

OligoNP's were produced accordingly to a procedure previously described in the literature (Aslam, Fu *et al.,* 2004). Aslam and collaborators made use of this method to produce gold nanoparticles using the multifunctional molecule oleyl amine (OLA), that electrostatically interacts with aqueous chloroaurate ions, reduces them, and subsequently stabilizes the nanoparticles formed (Aslam, Fu *et al.,* 2004). According to this and considering that the molecular structure of oligoaziridine is composed of several amines, three different concentrations of oligoaziridine (0,372mg/mL, 0,00372mg/mL and 0,00745mg/mL) were used, in order to check the formation of this type of gold nanoparticles, also referred as OligoNP's. OligoNP's_1 were formed by the addition of the highest oligoaziridine concentration (0,372mg/mL). This concentration lead to the formation of nanoparticles with sizes ranging from 134 to 286nm (Figure 7C). For the lower oligoaziridine's concentrations, it was possible to verify that the particles tend to aggregate, and do not allow the production of spherical nanoparticles. For 0,0372 mg/mL oligoaziridine's concentration (OligoNP's_2) merely a few nanoparticles were produced with average size of 140nm (Figure 7D). For oligoaziridine concentration of 0,00745mg/mL only aggregates were achieve. These results are in agreement to those previously reported by Aslam and colleagues, since their findings also

suggested that lowering OLA's concentration, would contribute for the production of well-defined aggregated particles.

Subsequently, MAL-PEG-MAL was grafted onto the surface of AuNP's_F. AuNP's_PEG were produced in several different ratios of PEG:AuNP's_F (500:1; 750:1; 1000:1; 2500:1; 5000:1; 10000:1). SEM images of all the nanoparticles produced in all the different ratios were collected. Through the analyses of the results, it was noticed that only the two last ratios were the ones with which was possible to obtain spherical nanoparticles with averages sizes of 140nm. However, there was also a lot of non-reactive material, which led us to lowering PEG's concentration from 0,1mg/mL to 0,02mg/mL. It was possible to verify that lowering PEG's concentration only induced particles formation in PEG: AuNP's ratio of 5000:1, with particles sizes ranging from 71 to 332nm (Figure 7E). However, particles with different sizes were obtained. The majority of the particles appear to have the size of the smallest ones referred (71nm).

Finally, oligoaziridine was added to AuNP'S_PEG, with the concentrations previously mentioned in the text. However the formation of spherical nanoparticles with sizes ranging from 75 to 151nm (Figure 7F) was only achieved with the highest concentration of the biosensor. The other two concentrations applied did not allow the production of spherical.

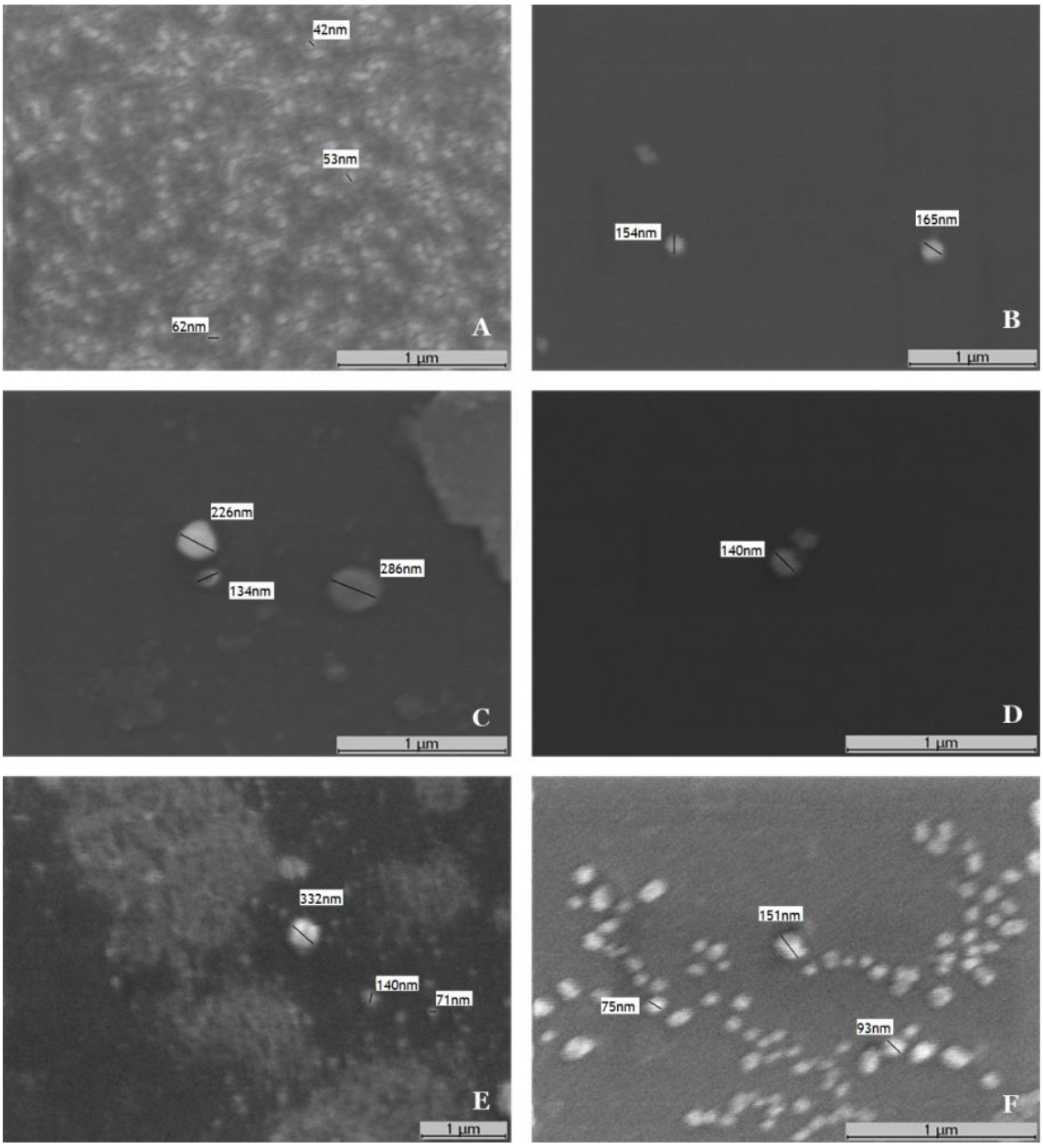

Figure 7 – SEM images of the produced nanoparticles: gold nanoparticles produced by method 1 (AuNP's_F) (A) original magnification 40.000x; gold nanoparticles coated with oligoaziridine concentration of 0,00745 mg/mL (Au_Oligo_3 nanoparticles) (B) original magnification 30.000x; gold nanoparticles produced by method 2 with oligoaziridine concentration of 0,372mg/mL (OligoNP's_1) (C) original magnification 40.000x; gold nanoparticles produced by method 2 with oligoaziridine concentration of 0,0372mg/mL OligoNP's_2 (D) original magnification 45.000x; gold nanoparticles coated with MAL-PEG-MAL (AuNP's_PEG) (E) original magnification 20.000x; gold nanoparticles coated with MAL-PEG-MAL and oligoaziridine(AuNP's_PEG_Oligo) (F) original magnification 45.000x.

3.2. Ultraviolet –Visible spectroscopy analysis

Once excited by electromagnetic radiation the electrons of metallic nanoparticles can easily make electronic transitions (Philip 2008). Colloidal solutions of gold nanoparticles are known to have a characteristic red color, which is due to their tiny dimensions (Huang and El-Sayed, 2010; Murphy *et al.,* 2008; Philip, 2008). As mentioned in chapter I, at the nanometer scale electrons oscillate on the particle surface and absorb electromagnetic radiation at a particular energy (Huang and El-Sayed, 2010). This SPR effect is not only a consequence of their small size, but is also caused by several factors, like solvent and surface functionalization. This dependence on surface effects make the surface plasmon an ideal monitor of adsorption of different molecules to particles surface, which allows nanoparticles assemblies to be used as sensing devices (Philip 2008). Considering these aspects, UV-VIS spectra of the nanoparticles produced, as well as the compounds used for their production were collected and are depicted in figure 8.

Figure 8A shows the UV-VIS spectra of the colloidal solution of gold nanoparticles with a characteristic peak at 523nm (Chen *et al.,* 2008)

When developing oligoaziridine, Vivek and collaborators stated the presence of 3 absorption bands with a maximum absorbance at 370nm. Figure 8B shows the three different concentrations of oligoaziridine used in this experiment. The black line refers to oligoaziridine first concentration 0,372mg/mL (B1). The green spectrum was obtained with a concentration of 0,0372mg/mL (B2) and the blue one 0,00745mg/mL (B3). As a consequence of lowering oligoaziridine concentrations, the absorbance register for the peaks, also decreases and the absorption bands become less defined. All three different oligoaziridine concentrations exhibit peaks approximately at 631nm, 560nm and 370nm (B3 shows a peak at 365nm). The first and second concentration also denote a well define peak at 391nm. B2 also shows a peak at 718 nm and B3 at 677 nm. Considering the absorption band at 370nm as a characteristic one for oligoaziridine, the other observed peaks may be due to the interaction between oligoaziridine and cell culture medium, used to dissolve the biosensor.

Figure 8C shows the UV-VIS spectrum of Au_Oligo, i.e., gold nanoparticles produced by method 1 coated with oligoaziridine. Both particles produced by this method present peaks at approximately 631nm and 390 nm. In both spectra of Au_Oligo_1 and Au_Oligo_2 (gold nanoparticles coated with oligoaziridine concentrations of 0,0372mg/mL and 0,00745mg/mL respectively), it is also possible to notice the absorption band at 370nm, characteristic of oligoaziridine. Less representative peaks are also observed in both spectra of Au_Oligo. These variations of absorbance are due to the interaction between gold nanoparticles and oligoaziridine, which causes a shift in the absorption bands of the original oligoaziridine spectra.

As it is possible to notice, gold nanoparticles characteristic absorption band do not appear in none of the spectra, demonstrating that all nanoparticles were covered by oligoaziridine.

OligoNP's (gold nanoparticles produced by method 2) are presented in Figure 8D. Only OligoNP's_1 particles (produced with a concentration of 0,372mg/mL) showed the absorbance peaks at 718nm, 521nm, 393nm and 372nm. The peak at 521nm reveals the formation of gold nanoparticles according to the method used, as described by Aslam and colleagues (Aslam *et al.,* 2004). The others peaks observed in the UV-VIS spectra are associated to oligoaziridine presence. For lower concentrations of oligoaziridine no characteristic peaks of gold nanoparticles or oligoaziridine ones were observed.

Figure 8E shows the MAL-PEG-MAL spectra at the concentration of 0,02mg/mL. MAL-PEG-MAL bounded to gold nanoparticles is shown that in figure 8F. It is possible to verify that the absorption band of gold nanoparticles suffered a slightly shift of 3nm to the right and that gold nanoparticles absorbance has diminished. PEG presence is also noticed at 686nm.

Oligoaziridine was also grafted onto the pre formed AuNP'S_PEG at a concentration of 0,372mg/mL (AuNP's_PEG_Oligo) and UV-VIS spectrum was acquired (Figure 8G). This spectrum presents absorption peaks at 733nm, 682nm, 390nm and 371nm. Comparing AuNP's_PEG_Oligo spectra with AuNP's_PEG one, it is possible to notice that the peak observed at 682nm in the first spectra, corresponds to the PEG absorption peak observed in the second one. The other peaks belong to the biosensor, as previously discussed. These features prove both the presence of oligoaziridine and PEG in the sample. AuNP's_F appear to be covered both with PEG and oligoaziridine. PEG also appears to be coated with this newly biosensor, since its absorbance has suffered a large decrease when compared to the spectrum of figure F.

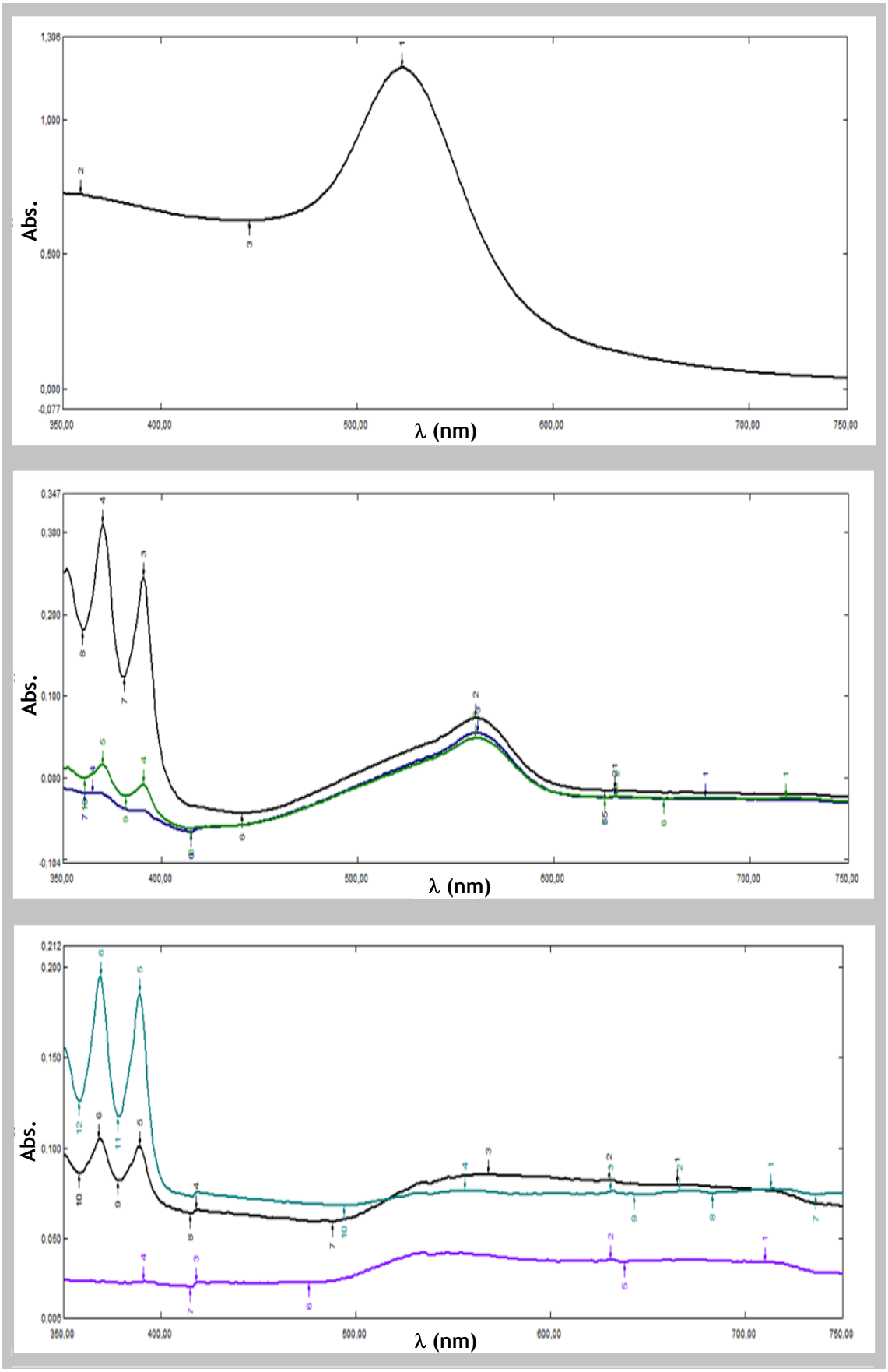
Abs.
λ (nm)
Abs.
λ (nm)
Abs.
λ (nm)

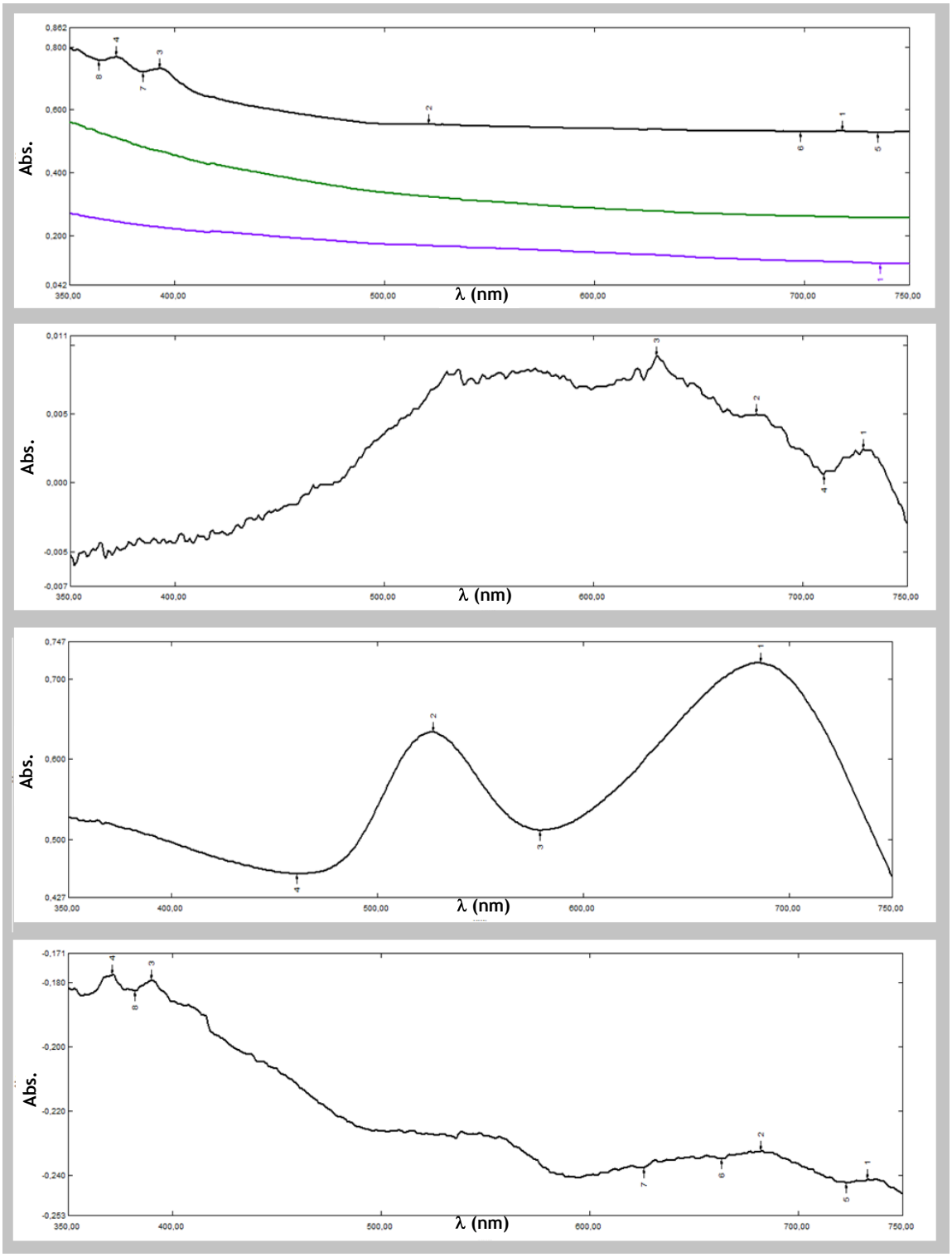

Figure 8 – UV-VIS spectra of the produced nanoparticles and the compounds used for their production: gold nanoparticles produced according method 1 (AuNP's_F) (A)-; overall spectra of Oligoaziridine with concentrations 0,372 mg/mL; 0,0372mg/mL; 0,00745mg/mL (black line, green line and blue line respectively) (B); overall spectra of gold nanoparticles coated with the same three different concentrations of oligoaziridine (Au_Oligo nanoparticles: blue line – Au_Oligo_1, black line – Au_Oligo_2; purple line – Au_Oligo_3) (C); overall spectra of gold nanoparticles produced according to method 2, again with the same 3 different oligoaziridine's concentration (OligoNP's particles: black line – OligoNP's_1; green line – OligoNP's_2; purple line OligoNP's_3) (D); PEG solution concentration 0,02mg/mL (E); Gold nanoparticles produced by method 1 coated with PEG (AuNP's_PEG) (F); gold nanoparticles produced by method 1 coated with PEG and Oligoaziridine (AuNP's_PEG_Oligo) (G).

3.3. FTIR – analysis of the nanoparticles

FTIR was used to characterize the nanoparticles produced with and without oligoaziridine addition, as well as the effect of PEG to AuNP's_F.

As previously mentioned, amine derivates complex with gold nanoparticles in a similar manner to that of thiol derivates (Nelson and Rothberg 2011; Selvakannan *et al.,* 2003). These differences in gold nanoparticles affinities for adhesion is a result of the different surface charge due to the synthesis conditions employed (Kim and Yi 2008). For instance, AuNP's_F show good adhesion properties for amine moieties when citrate is used as a reductive agent and also as a capping agent. These features are conferred from the high temperature applied to the reaction when producing the particles (Jana *et al.,* 2001; Kim and Yi 2008). The seed method, for example, makes use of $NaBH_4$ and uses citrate only as a capping agent of the particles, as the reaction is performed at room temperature (Jana *et al.,* 2001; Kim and Yi 2008). Gold nanoparticles produced by this method present good affinity for thiol groups (Jana *et al.,* 2001; Kim and Yi 2008). As a result, the surface of AuNP for immobilization can be modified according to the functional moiety of the initial substrate (Jana *et al.,* 2001; Kim and Yi 2008).

Having in consideration the chemical structures of both oligoaziridine (Figure 9A) and MAL-PEG-MAL (Figure 9B) it is easily understandable that these two compounds can interact with gold nanoparticles as they both present derivates amines in their chemical structures.

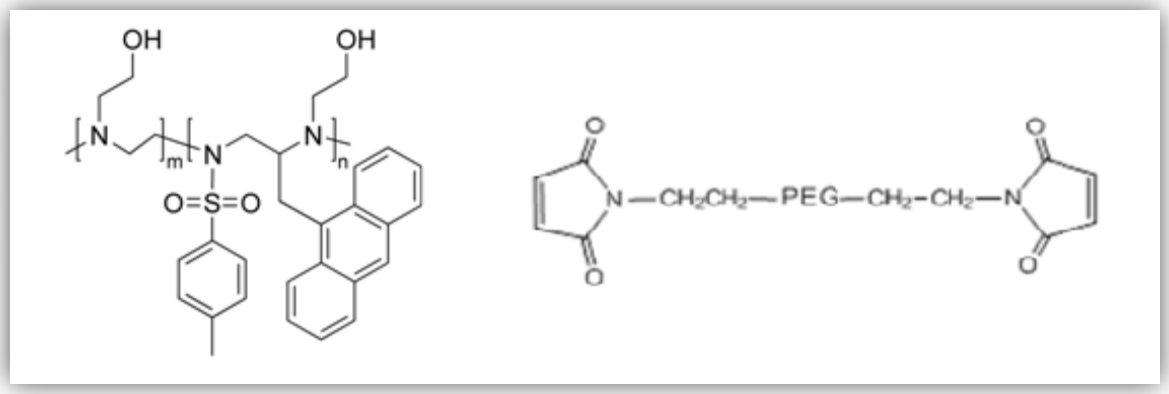

Figure 9 – Representation of the structure of oligoaziridine (A) and MAL-PEG—MAL (B) (Adapted from Raje *et al.,* submitted manuscript).

Oligoaziridine was not only grafted onto AuNP's_F surface but also to the formed AuNP's_PEG, in order to evaluate their entry into cells environment by fluorescence assays. Maleimide group is known for its ability to interact with sulfur atoms (Aversa *et al.,* 2005). Again, considering both structures presented in figure 9, interactions between maleimide and oligoaziridine are likely to happen due to presence of the tosyl group (Aversa *et al.,* 2005).

It is important to clarify that MAL-PEG-MAL was not attached to gold nanoparticles when they were produced by method 2, due to the lack of oligoaziridine.

Figure 10 show different FTIR spectra of the compounds used as well as the nanoparticles produced. In both spectra, the peaks with higher absorbance were carefully analyzed according to the data reported in the literature (Lambert *et al.*, 1998). Atoms stretch and deformations are presented in the spectra and were used to confirm the chemical structures of the produced nanoparticles as well as the compounds used.

Gold nanoparticles produced by method 1 (figure 10A) present the vibrational peak for N=C=N (frequency range 2150–2100cm^{-1} as well as ring stretches (frequency range 1615 – 1565 cm^{-1}) and CH stretches (frequency range 2990 – 2850 cm^{-1}) and deformations (frequency range 1400 – 1370 cm^{-1}) as previously described in the literature (Lambert *et al.*, 1998). Nitrogen atoms presence does correlate with this particles affinity to amine moieties.

When analyzing oligoaziridine spectrum (figure 10B) it can be identified the presence of C-H, C-N, C-O and SO_2 (frequency range 1170-1145cm^{-1}) stretches and CH_2 deformations, as shown by the chemical structure of this compound (figure 9).

The MAL-PEG-MAL spectrum (figure 10C) shows some noise due to the low concentration used. Again, as expected, C-H and C-N stretches as well as CH_2 and CH deformation are marked in the figure.

Au_Oligo_3 (figure 10D) and OligoNp's_1 (figure 10E) FTIR spectra, demonstrate that oligoaziridine binds to gold nanoparticles. Through the analysis of FTIR spectra of Au_Oligo_3 it is possible to notice that the N=C=N peak from AuNP's_F disappears. Therefore, it can be concluded that the linkage between nanoparticles and oligoaziridine does occurs by breaking N=C=N bond, confirming again, the AuNP's_F affinity for nitrogen atoms. It can also be concluded that SO_2 from oligoaziridine stays at the surface of the produced nanoparticles as can be seen in the spectra (figure 10D).

OligoNp's_1 (particles formed by the addition of oligoaziridine to gold solution) also present C-H, C=O, SO_2, NH_3^+ and R-C-O stretches as well as NH_2 deformation. Its spectrum is quite similar to that of SH3 nanoparticles (figure 10E).

FTIR spectrum of PEG coupled to AuNP's_F is presented in figure 10G. Again, since the N=C=N stretch from gold nanoparticles disappears with PEG addition, it is suitable to assure that the bounding between this two compounds occurred due to AuNP's_F affinity to amines, as previously discussed in the text.

Finally, after oligoaziridine addition to AuNP's_PEG, FTIR spectrum was also collected (Figure 10H). Since no SO_2 peak was observed, it can also be concluded that this group is responsible for the interaction between the maleimide group of PEG and oligoaziridine which proves the between AuNP's_PEG to oligoaziridine (AuNP'S_PEG_Oligo).

For the sake of simplicity, figure 10F shows the overall spectra of AuNP's_F, oligoaziridine, Au_Oligo_3 and OligoNP's_1 particles, and figure 10I displays the overall spectra of AuNP's_F, Oligoaziridine, MAL-PEG-MAL, AuNP's_PEG and AuNP's_PEG_Oligo, which

allows a better understanding of the changes occurred in the spectra of the different samples.

It can also be noticed in the majority of the spectra a band with a frequency range (3700–3600nm) (Lambert *et al.,* 1998) related with OH deformation. These specifics peaks are likely due to water and ethanol contaminations when cleaning the diamond crystal between the experiments. Some of the spectra also show CO_2 contamination, carefully indicated in the spectra.

In conclusion, FTIR spectra were collected and carefully analyzed in order to prove that PEG is bound to AuNP's_F and also show oligoaziridine linkage to AuNP's_F and AuNP's_PEG.

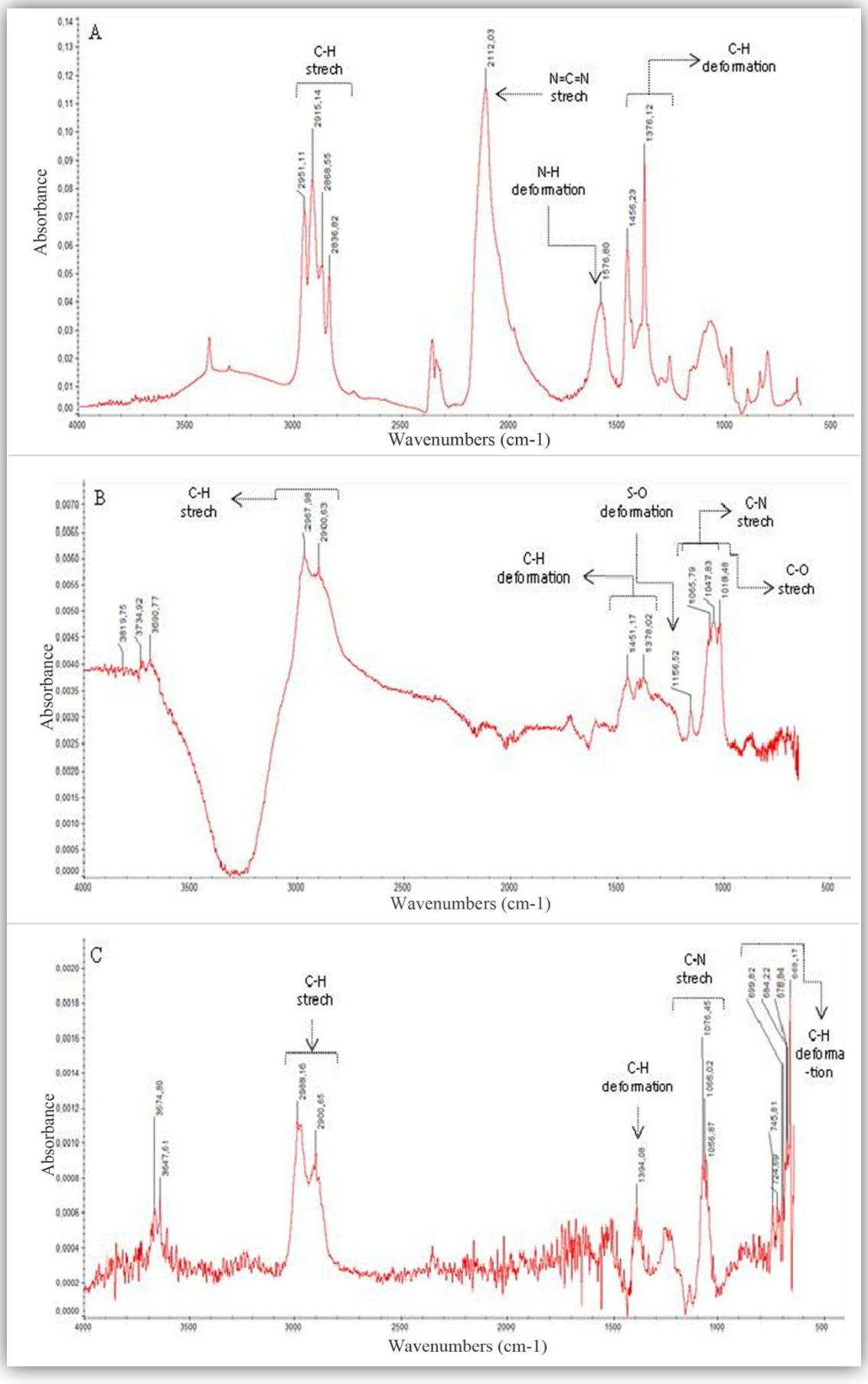
A
C-H strech
N=C=N strech
C-H deformation
N-H deformation
2112,03
2915,14
2951,11
2868,55
2836,82
1376,80
1456,23
1376,12
Absorbance
Wavenumbers (cm-1)
B
C-H strech
S-O deformation
C-N strech
C-H deformation
C-O strech
2967,98
2900,63
3819,75
3734,92
3690,77
1451,17
1378,02
1156,52
1065,79
1047,83
1018,48
Absorbance
Wavenumbers (cm-1)
C
C-H strech
C-N strech
C-H deformation
C-H deforma-tion
2888,16
2900,65
3674,80
3647,61
1394,08
1076,45
1066,02
1056,87
745,81
724,69
699,82
684,22
678,84
669,17
Absorbance
Wavenumbers (cm-1)

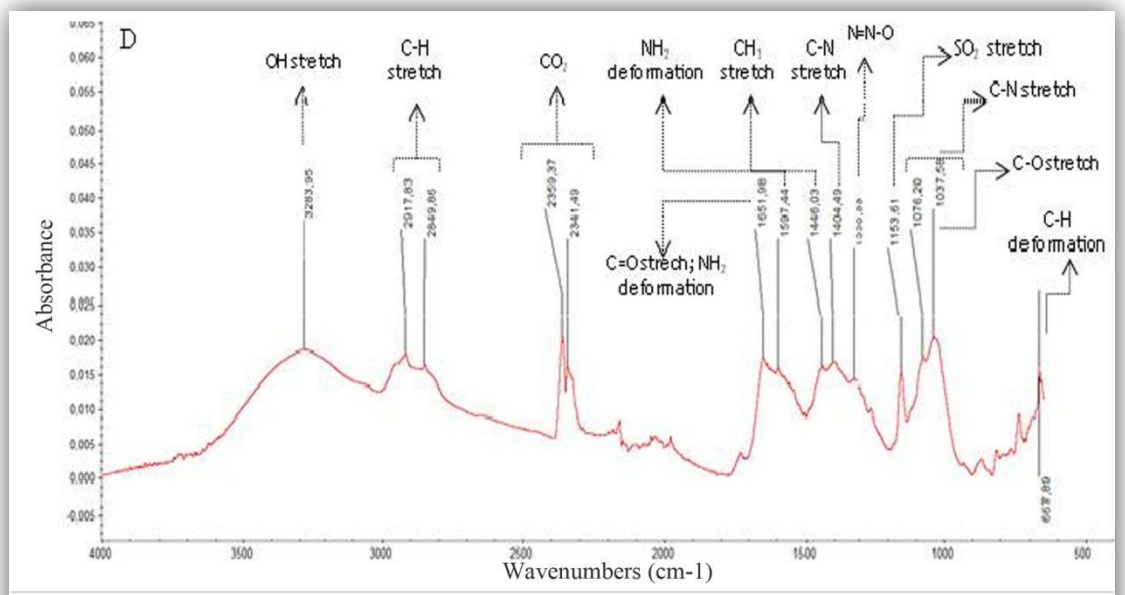
D
OH stretch
C-H stretch
CO2
NH2 deformation
CH3 stretch
C-N stretch
N=N-O
SO2 stretch
C-N stretch
C-O stretch
C-H deformation
C=O stretch; NH2 deformation
Absorbance
Wavenumbers (cm-1)

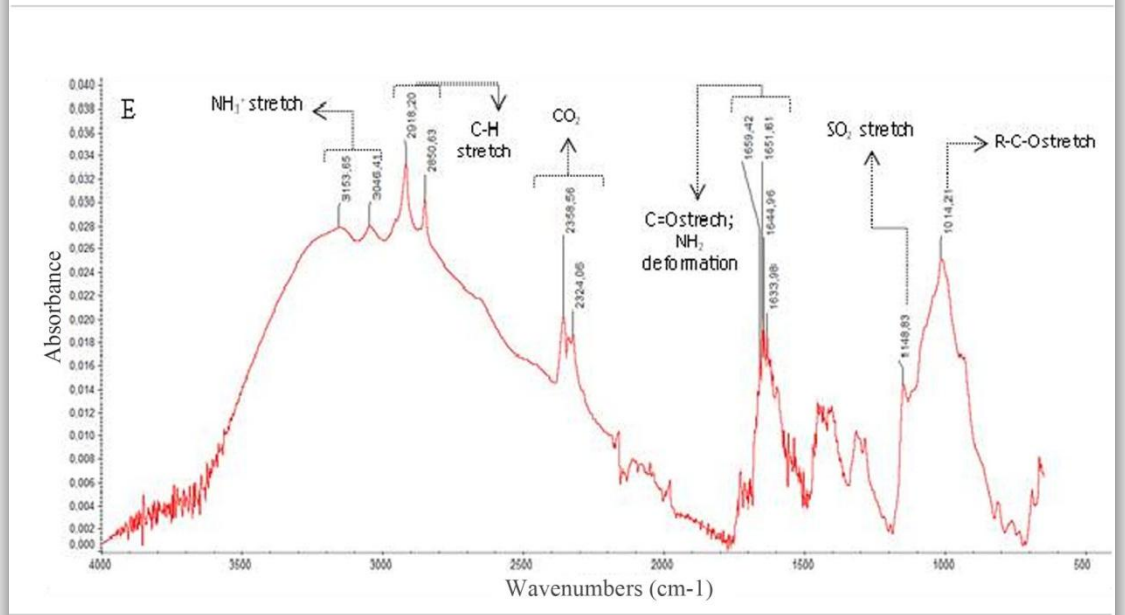
E
NH3+ stretch
C-H stretch
CO2
C=O stretch; NH2 deformation
SO2 stretch
R-C-O stretch
Absorbance
Wavenumbers (cm-1)

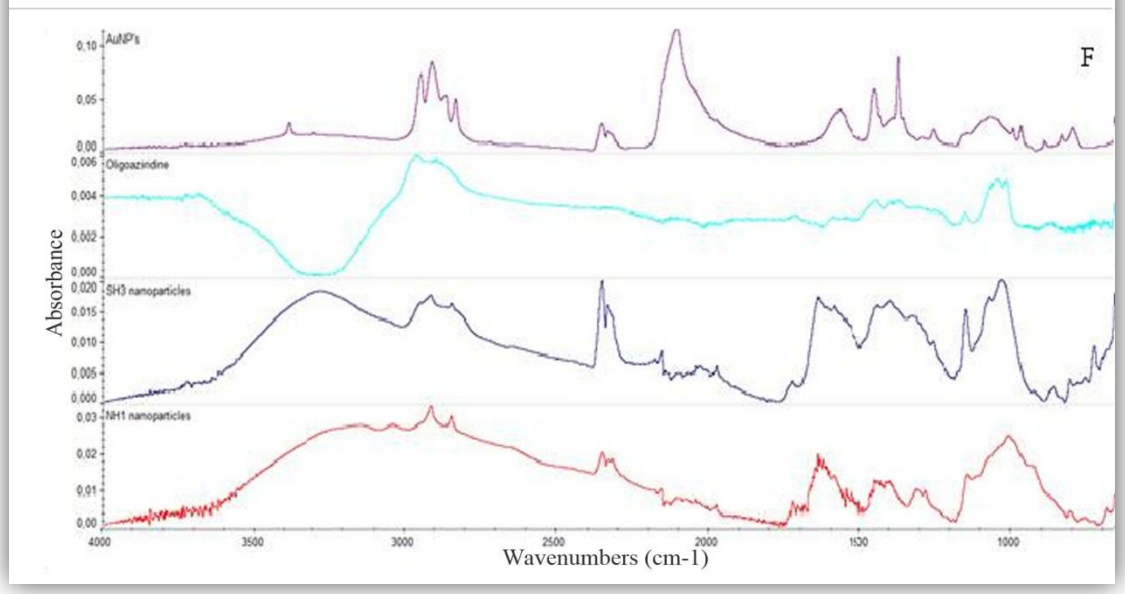
F
AuNP's
Oligoazinidine
SH3 nanoparticles
NH1 nanoparticles
Absorbance
Wavenumbers (cm-1)

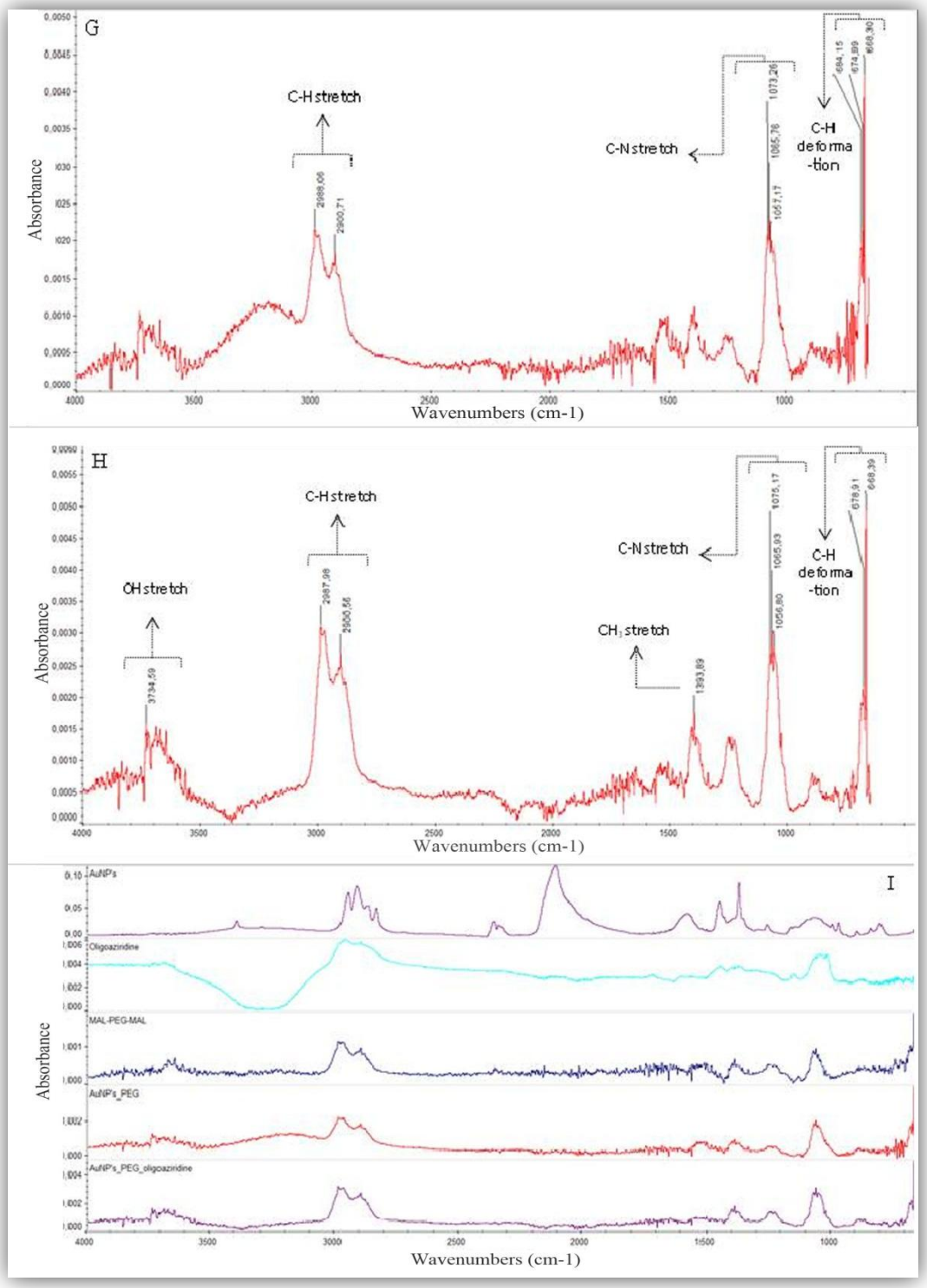

Figure 10 - FTIR spectra of the produced nanoparticles and the compounds used for their porduction: gold nanoparticles produced by method 1 (AuNP's_F) (A); Oligoaziridine (B); MAL-PEG-MAL (C); gold nanoparticles produced by method 1 coated with oligoaziridine concentration of 0,00745mg/mL (Au_Oligo_3) (D);Gold nanoparticles produced by method 2 with oligoaziridine concentration of 0,372mg/mL (OligoNP's_1) (E); General specta of A, B, D and E (F); gold nanoparticles produced by method 1 coated with MAL-PEG-MAL (AuNP's_PEG) (G); gold nanoparticles coated with MAL-PEG-MAL and oligoaziridine concentration of 0,372mg/mL (AuNP's_PEG_Oligoaziridine) (H); General spectra of A,B,C,G and H (I).

3.4. X-Ray Diffraction analysis

In order to prove the production of AuNP's_PEG (gold nanoparticles produced by method 1 coated with MAL-PEG-MAL), a XRD spectra was collected and carefully analyzed (Figure 11). Freeze dried samples of AuN's_F as well as MAL-PEG-MAL were used as controls. When capping AuNP's with PEG, it can be seen that both characteristic peaks of these constituents suffer a shift, i.e., there is a phase transformation which demonstrate a new crystalline rearrangement and therefore the formation of a new crystalline compound.

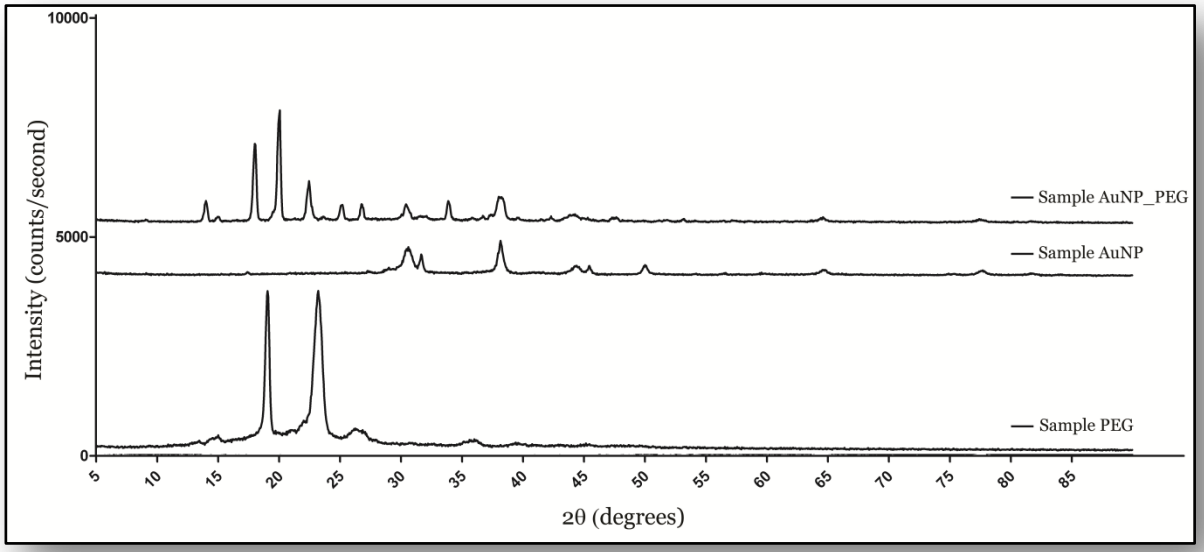

Figure 11 – XRD spectra of gold nanoparticles produced by method 1, MAL-PEG-MAL and gold nanoparticles coated with PEG (AuNP's_PEG).

3.5. Qualitative Evaluation of *in vitro* transfection

In order to prove that nanoparticles enter into the cells, A549 cells were transfected with the produced nanoparticles and immunofluorescence (figure 12) and CLSM images (figure 13) were obtained. A549 cells were transfected with Oligoaziridine, Au_Oligo_3, OligoNP's_1 and AuNP's_PEG_Oligo. From immunofluorescence images it can be seen that Oligoaziridine (Figure 12A) does enter within the cells in a disperse manner, when compared to the ones transfected with nanoparticles. Transfected cells with Au_Oligo_3, OligoNP's_1 and AuNP's_PEG_Oligo are shown in figures 12B, 12C and 12D, respectively. Nanoparticles are easily observed in both images and appear to cross cytoplasmatic membrane.

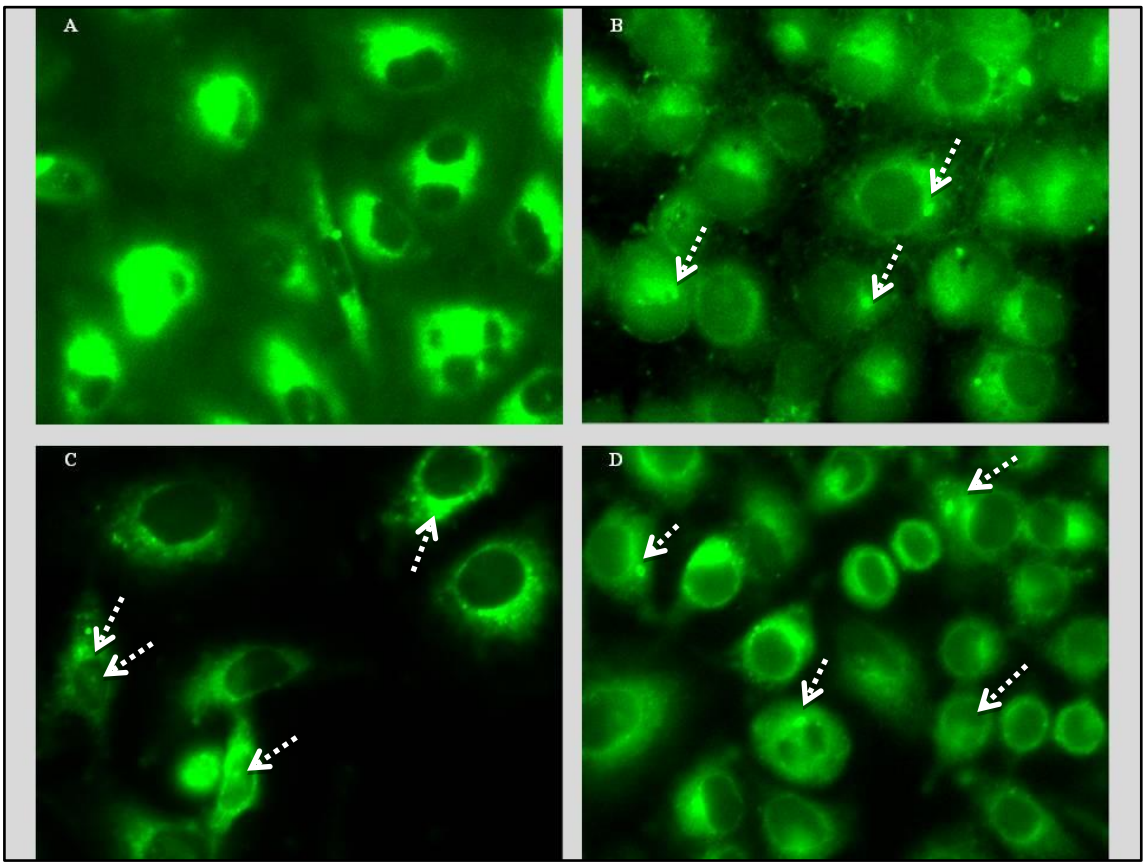

Figure 12 – Immunofluorescence images of A449 cells transfected with oligoaziridine (A); Gold nanoparticles coated with oligoaziridine concentration of 0,00745mg/mL (Au_Oligo_3) (B); Gold nanoparticles produced by method 2 with oligoaziridine concentration of 0,372mg/mL (OligoNP's_1) (C); and gold nanoparticles coated with PEG and oligoaziridine concentration of 0,372mg/mL (AuNP's_PEG_Oligo) (D). Original magnification x63.

However, for better understanding of the particles' cell location, CLSM images were also collected.

CLSM allows the obtention of images with higher resolution than immunofluorescence microscopy (Van Gough 2008). A general problem associated with fluorescence microscopy is that the illumination used to excite the sample covers its entire thickness, which leads to

data convoluted with light originating from outside the region of interest. CLSM does overcome this specific difficulty by using a focused laser beam that reaches the sample, collecting the reflected or emitted light, while removing any light coming from the outside of the focal point of the laser beam (Van Gough 2008). CLSM can collect images of individual slices using fluorescence or reflection from sample in the xy, xz and yz planes. Collecting individual slices in the xy plane with small steps in the z-direction provides all the information necessary to perform a 3-D reconstruction of the interior of a sample (Van Gough 2008). Although this type of reconstruction can be performed using CT or transmission electron microscopy (TEM) in concern to tomography, both of these techniques present some disadvantages. In CT biological samples lack the z-contrast necessary to resolve the internal structures through interaction with x-rays. This procedure also, in addition to the long analysis times (hours to days); TEM tomography on the other hand requires freezing of the samples in order to place aqueous, biological samples into an ultra-high vacuum and requires (potentially toxic) heavy metal dying, both of which remove the ability to observe changes in one sample over time (Van Gough 2008).

As so, the collected CLSM images (Figure 13) give a clear idea of the particles location within the cells. In this figure, the left column shows the 2D view of the transfected cells with the different compounds, while the right column presents the 3D view.

Again, oligoaziridine transfection images (figure 13 A and B) demonstrated the dispersion of the biosensor within the cell. Images from cell transfection with Au_Oligo_3 (figure 13 C and D) show that not all particles entered within the cells. However, it also shows that some particles did actually enter into the cell nucleus while others remained in the cytoplasm, giving an idea of nanoparticles sizes dispersion.

Some OligoNP's_1 (figure 13 E and F) appear to have cross cytoplasmatic membrane and reached the nucleus, while others stayed in the surrounding of the cytoplasmatic membrane, as a consequence of their larger size.

Finally, cells transfected with AuNP's_PEG_Oligo (figure 13G and H) were marked with nanoparticles in and outside cell nucleus. As already expected AuNP's_PEG_Oligo were the nanoparticles that have shown the better transfection into cell nucleus. This can be explained by their relative small size as well as the presence of PEG layer that takes advantage of the EPR cancer cells.

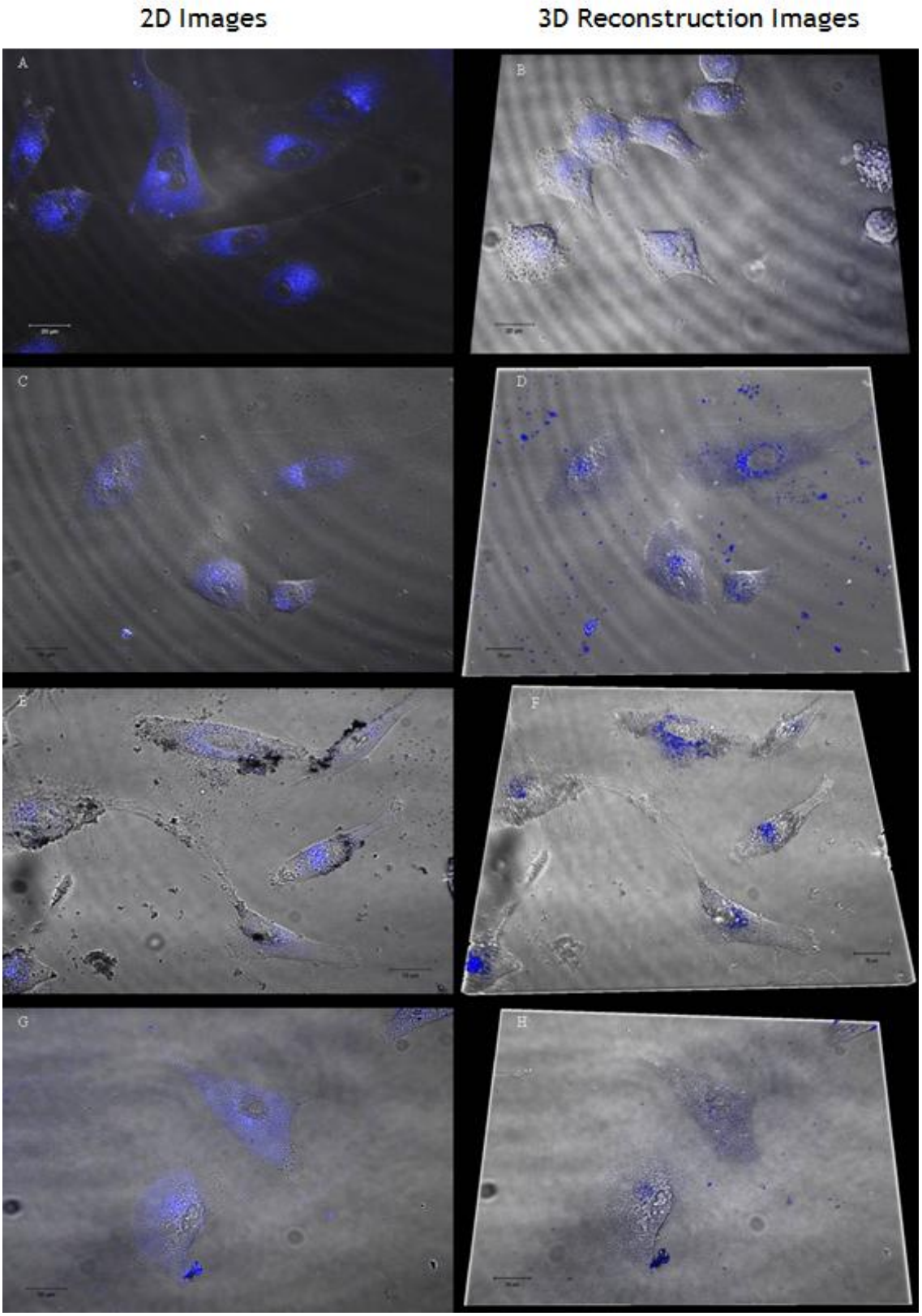

Figure 13 – CLSM images of A449 cells transfected with oligoaziridine (A); gold nanoparticles produced by method 1 coated with oligoaziridine concentration of 0,00745mg/mL (Au_Oligo_3) (C); gold nanoparticles produced by method 2 with oligoaziridine concentration of 0,372mg/mL (OligoNp's_1) (E); Gold nanoparticles produced by method 1 conated with MAL-PEG-MAL and oligoaziridine concentration of 0,372mg/mL (AuNP's_PEG_Oligo) (G); and CLSM 3D reconstruction images of A449 cells transfected with oligoaziridine (B); gold nanoparticles produced by method 1 coated with oligoaziridine concentration of 0,00745mg/mL (Au_Oligo_3) (D); gold nanoparticles produced by method 2 with oligoaziridine concentration of 0,372mg/mL (OligoNp's_1) (F); Gold nanoparticles produced by method 1 coated with MAL-PEG-MAL and oligoaziridine concentration of 0,372mg/mL (AuNP's_PEG_Oligo) (H). Original magnification x40.

3.6. Evaluation of the cytotoxic profile of the produced nanoparticles

The cytocompability of gold nanoparticles produced herein was characterized through *in vitro* studies.

In literature there are different studies reporting conflicting data about gold nanoparticles cytotoxicity (Schleh *et al.*, 2011). Even so, AuNP's are usually considered to be biocompatible (Schleh *et al.,* 2011; Chen *et al.,* 2008). Nevertheless, the size similarity of gold nanoparticles to biological molecules can lead to undesired cellular entry jeopardizing normal cellular function (Chen *et al.,* 2008). This specific concern has been the target of several studies aiming to provide a better insight about their toxicity profile (Chen *et al.,* 2008; Murphy *et al.,* 2008). While some authors studied size dependent toxicity, others investigated surface charge influence. In 2007, Pan and colleagues found that gold nanoparticles with sizes ranging from 1 to 2 nm were cytotoxic, while 15nm were not. These results appeared to confirm other results previously obtained about size dependent toxicity of this type of particles (Pan 2007; Chen *et al.,* 2008). On the other hand, Rotello and colleagues proved that cationic chains appear to present moderate cytotoxicity as anionic side chains were generally nontoxic (Goodman *et al.,* 2004; Chen *et al.,* 2008).

Oligoaziridine cytotoxicity was previously studied by our group and the results are discussed in a manuscript submitted for publication. The MTS assay results obtained suggested that no changes occur in cell viability, proving no acute cytotoxic effect of the biosensor. As previously mention in sub section 2.2.11, A549 small lung cancer cells were seeded at the same initial density in a 96-well plates, with or without compounds to assess its cytotoxicity. Cell adhesion and proliferation was observed (Figure 14) in wells where cells were in contact with the compounds and nanoparticles and in the negative control (K-). In the positive control neither cell adhesion nor proliferation were observed. Dead cells with their characteristic can also be seen in figure 14 as K+.

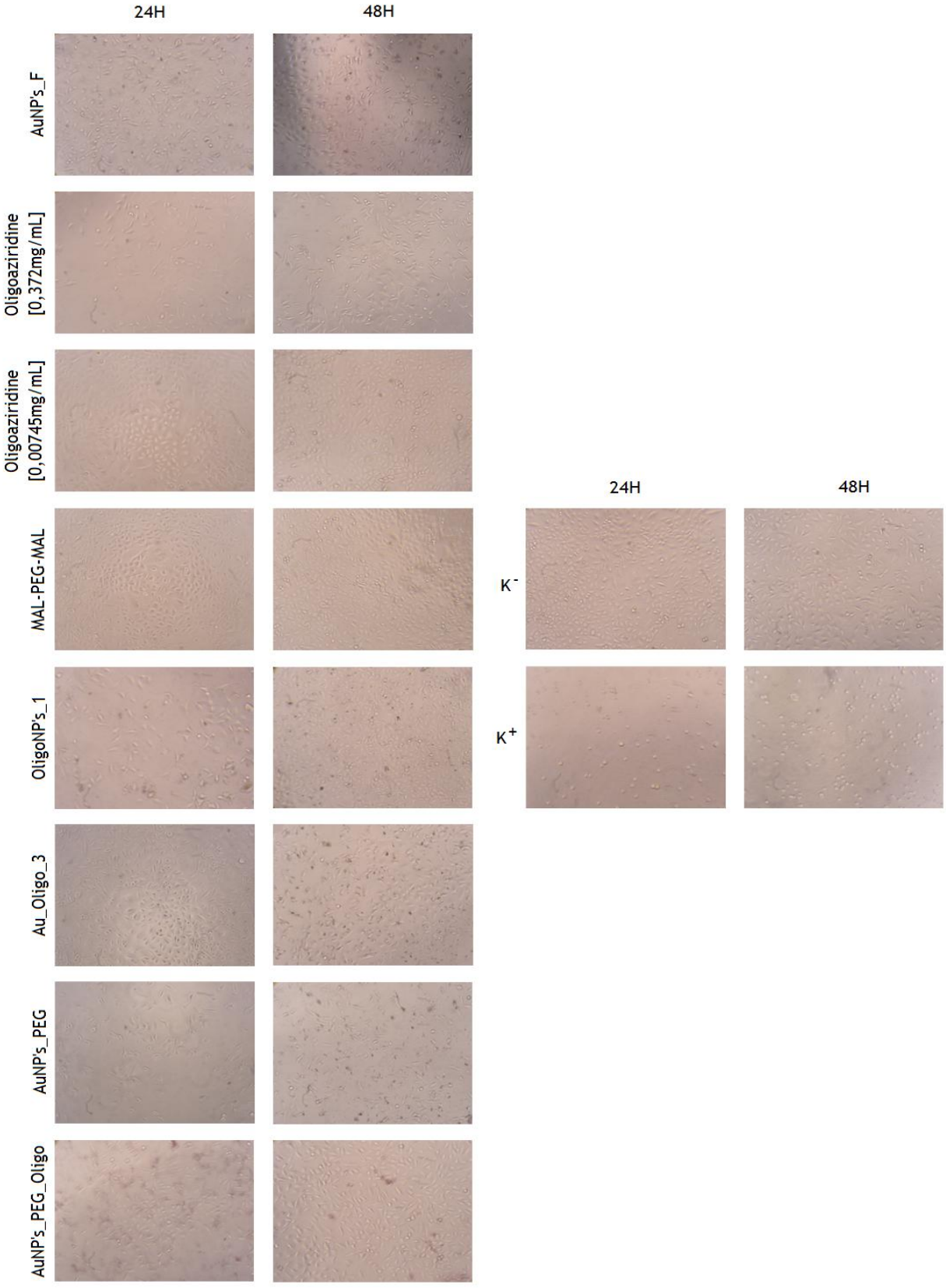

Figure 14 –Inverted Microscope Images of A549 cells in contact with: gold nanoparticles produced by method 1 (AuNp's_F); Oligoaziridine (concentration = 0,372mg/mL); Oligoaziridine (concentration = 0,00745mg/mL); Mal-PEG-Mal; gold nanoparticles produced by method 2 with oligoaziridine concentration of 0,372mg/mL (OligoNPs_1); gold nanoparticles produced by method 1 coated with oligoaziridine concentration of 0,00745mg/mL (Au_Oligo_3); gold nanoparticles produced by method 1 coated with MAL-PEG-MAL (AuNP's_PEG); Gold nanoparticles produced by method 1 coated with MAL-PEG-MAL and oligoaziridine concentration of 0,372mg/mL (AuNp's_PEG_Oligo); negative control (K^-); positive control (K^+). Original magnification x100.

The MTS assay results confirmed what was observed through the optical microscopy images. It was also proved that cells in contact with the nanoparticles showed higher cell viability than the positive control but lower than that of the negative control, during the 48 hours of incubation. The positive control (K^+) showed no viable cells. Non standing, the results obtained using this assay proved that compounds used in order to produce nanoparticles, as well as the nanoparticles *per se*, did not affected cell viability. The assay showed a significant difference between positive control ($p< 0,05$) and the negative control and cells exposed to the different compounds and nanoparticles after 24 ($^*p< 0,05$) and 48 hours ($^{\#}p< 0,05$) of incubation (Figure 15). Based on the results obtained it is possible to say that nanoparticles herein produced do not have an acute cytotoxic effect and they are good candidates to be used in future biomedical applications.

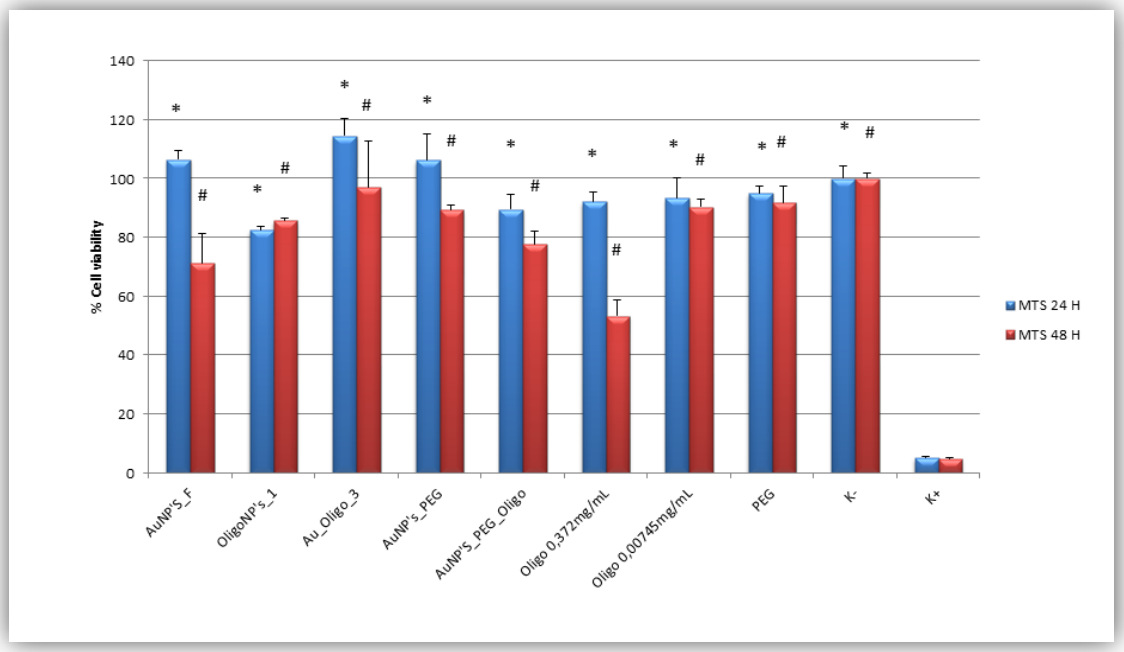

Figure 15 - Cellular activities measured by the MTS assay after 24h (blue columns) and 48h (red columns) in contact with the compounds and nanoparticles produced. Gold nanoparticles produced by method 1 (AuNP's_F); Gold nanoparticles produced by method 2 with oligoaziridine concentration of 0,372mg/mL (OligoNp's_1); Gold nanoparticles produced by method 1 coated with oligoaziridine concentration of 0,00745mg/mL (Au_Oligo_3); Gold nanoparticles produced by method 1 coated with MAL-PEG-MAL (AuNP's_PEG); Gold nanoparticles produced by method 1 coated with MAL-PEG-MAL and oligoaziridine concentration of 0,372mg/mL (AuNP's_PEG_Oligo); Oligoaziridine concentration of 0,372mg/mL; Oligoaziridine concentration of 0,00745mg/mL; MAL-PEG-MAL concentration of 0,02mg/mL; Negative control (K^-); positive control (K^+). Each result is mean ± standard error of the mean of at least three independent experiments. Statistical analyses was performed using one-way ANOVA with Dunet's post hoc test ($^*p<0,05$ and $^{\#}p<0,05$)

Chapter IV – Conclusions and Futures Perspectives

4. Conclusion and Future Perspectives

Multifunctional nanoparticles hold a great promise for cancer treatment. They can detect cancer in an early stage and make the delivery of suitable therapeutic agents more efficient.

In the present study two different methods were used to produce gold nanoparticles. It was noticed that depending on the method used, they can interact with different types of molecules. Five types of nanoparticles were successfully produced herein: AuNP's_F; Au_Oligo_3; OligoNP's_1; AuNP's_PEG; and AuNP's_PEG_Oligo. All nanoparticles synthesis involved the use of a stabilizing agent, in order to prevent nanoparticles aggregation. MAL-PEG-MAL was attached to AuNP's_F in order to enhance blood circulation time, by preventing their interaction with plasma proteins and by inhibiting the system of opsonises involved in its uptake by macrophages. Nanoparticles coated with PEG also take advantage from EPR effect of cancer cells, due to their hydrophobic domain.

SEM, UV-VIS and FTIR and XRD analysis were performed in order to analyze nanoparticles morphology, assembly and chemical composition. The binding of MAL-PEG-MAL to the different nanoparticles was confirmed by XRD, which was fundamental for the purpose of this work.

Proliferation studies of A549 cells in contact with the nanodevices herein produced were also performed. The results obtained revealed cell adhesion and proliferation in the presence of the nanoparticles. Subsequently, cells were transfected with oligoaziridine, Au_Oligo_3, OligoNP's_1 and AuNP's_PEG_Oligo. The results of *in vitro* transfections were evaluated through immunofluorescence and CLSM assays. According to the images obtained from both immunofluorescence and CLSM assays it was possible to conclude that the produced nanoparticles do enter within cancer cells and also appear to target cells nucleus. Moreover, the cytotoxic assays demonstrated that both compounds and nanoparticles are biocompatible and open new doors for its future application in the biomedical field.

The nanoparticles made from or coated with oligoaziridine will offer the opportunity of exploiting both cancer imaging and guided hyperthermia therapy. For instance, AuNP's_PEG_Oligo will also be conjugated with a specific cell-binding sequence YIGRS, that are recognized by cancer cells, in order to improve cancer cells uptake. OligoNP's will also be coated with PEG and the same EMC proteins will be applied to these nanoparticles. Furthermore, both types of particles will be also conjugated will paclitaxel, one of the chemotherapeutic agents widely used in cancer therapy. Once within cancer cell nucleus, nanoparticles will be able to exert their effect such as, delivery of drugs and genes or even induce apoptosis, without jeopardizing healthy tissues.

In order to evaluate nanoparticles exact location within cancer cells, specific probes that mark for cytoesqueleton and cell nucleus will also be used.

The ability of these systems to induce cell apoptosis through hyperthermia will also be evaluated by circular dichroism assay. Furthermore, the presence of oligoaziridine in the nanoparticles will allow us to track particles location inside cells.

These systems will be valuable candidates to improve in a near future the available cancer therapies.

Bibliography

5. Bibliography

Ahmed, F., R. I. Pakunlu, *et al.,* (2006). "Biodegradable polymersomes loaded with both paclitaxel and doxorubicin permeate and shrink tumors, inducing apoptosis in proportion to accumulated drug." Journal of Controlled Release 116(2), 150-158.

Akiyama, S. K., K. Olden, *et al.,* (1995). "Fibronectin and integrins in invasion and metastasis." Cancer and Metastasis Reviews 14(3), 173-189.

Akiyama, Y., T. Mori, *et al.,* (2009). "The effects of PEG grafting level and injection dose on gold nanorod biodistribution in the tumor-bearing mice." Journal of Controlled Release 139(1), 81-84.

Allen, C., N. Dos Santos, *et al.,* (2002). "Controlling the physical behavior and biological performance of liposome formulations through use of surface grafted poly (ethylene glycol)." Bioscience reports 22(2), 225-250.

Aslam, M., L. Fu, *et al.,* (2004). "Novel one-step synthesis of amine-stabilized aqueous colloidal gold nanoparticles." J. Mater. Chem. 14(12), 1795-1797.

Bacsik, Z., Mink, J., and Keresztury, G. (2004). FTIR Spectroscopy of the Atmosphere. I. Principles and Methods. Applied Spectroscopy Reviews (pp. 295-363).

Baldwin, A. D., and Kiick, K. L. (2010). Polysaccharide-modified synthetic polymeric biomaterials. Biopolymers, 94(1), 128-40..

Bhushan, B. (2010) "Introduction to Nanotechnology." Springer Handbook of Nanotechnology, 1-13.

Bode, A. M. and Z. Dong (2009). "Cancer prevention research—then and now." Nature Reviews Cancer 9(7), 508-516.

Brewer, E., Coleman, J., and Lowman, A. (2011). Emerging Technologies of Polymeric Nanoparticles in Cancer Drug Delivery. Journal of Nanomaterials, 2011, 1-10.

Brigger, I., C. Dubernet, *et al.,* (2002). "Nanoparticles in cancer therapy and diagnosis." Advanced drug delivery reviews 54(5), 631-651.

Chen, P. C., S. C. Mwakwari, *et al.,* (2008). "Gold nanoparticles: From nanomedicine to nanosensing." Nanotechnology, Science and Applications 1, 45-66.

Chertok, B., B. A. Moffat, *et al.,* (2008). "Iron oxide nanoparticles as a drug delivery vehicle for MRI monitored magnetic targeting of brain tumors." Biomaterials 29(4), 487-496.

Cherukuri, P., Glazer, E. S., and Curley, S. a. (2010). Targeted hyperthermia using metal nanoparticles. Advanced drug delivery reviews, 62(3), 339-45.

Cho, K., X. Wang, *et al.,* (2008). "Therapeutic nanoparticles for drug delivery in cancer." Clinical Cancer Research 14(5), 1310.

Choi, B.-H., Choi, Y. S., Kang, D. G., Kim, B. J., Song, Y. H., and Cha, H. J. (2010). Cell behavior on extracellular matrix mimic materials based on mussel adhesive protein fused with functional peptides. Biomaterials, 31(34), 8980-8.

Collins, K. (1997). The cell cycle and cancer. Proceedings of the National Academy of Sciences, 94(7), 2776-2778.

Croce, C. M. (2008). "Oncogenes and cancer." New England journal of medicine 358(5), 502-511.

Danhier, F., Feron, O., and Préat, V. (2010). To exploit the tumor microenvironment: Passive and active tumor targeting of nanocarriers for anti-cancer drug delivery. Journal of controlled release, 148(2), 135-146.

Davis, M. E. (2008). "Nanoparticle therapeutics: an emerging treatment modality for cancer." Nature Reviews Drug Discovery 7(9), 771-782.

Demirgo z, D., A. Garg, *et al.,* (2008). "PR_b-targeted PEGylated liposomes for prostate cancer therapy." Langmuir 24(23), 13518-13524.

Discher, D. E. and F. Ahmed (2006). "Polymersomes." Annu. Rev. Biomed. Eng. 8, 323-341.

Dong, X., and Mumper, R. J. (2010). Nanomedicinal strategies to treat multidrug-resistant tumors: current progress. Nanomedicine (London, England), 5(4), 597-615.

Fang, C., N. Bhattarai, *et al.,* (2009). "Functionalized Nanoparticles with Long Term Stability in Biological Media." Small 5(14), 1637-1641.

Farokhzad, O. C. and R. Langer (2009). "Impact of nanotechnology on drug delivery." ACS nano 3(1), 16-20.

Frens, G. (1973). "Controlled nucleation for the regulation of the particle size in monodisperse gold suspensions." Nature 241(105), 20-22.

Gaspar, V., F. Sousa, *et al.,* (2011) "Formulation of chitosan–TPP–pDNA nanocapsules for gene therapy applications." Nanotechnology 22, 015101.

Ghosh, P., G. Han, *et al.,* (2008). "Gold nanoparticles in delivery applications." Advanced drug delivery reviews 60(11), 1307-1315.

Goodman, C. M., C. D. McCusker, *et al.,* (2004). "Toxicity of gold nanoparticles functionalized with cationic and anionic side chains." Bioconjugate chemistry 15(4), 897-900.

Gunasekera, U. A., Q. A. Pankhurst, *et al.,* (2009). "Imaging applications of nanotechnology in cancer." Targeted oncology 4(3), 169-181.

Haley, B. and E. Frenkel (2008). Nanoparticles for drug delivery in cancer treatment, Elsevier.

Hanahan, D. (2000). "The hallmarks of cancer." Cell 100(1), 57-70.

Huang, X., and El-Sayed, M. a. (2010). Gold nanoparticles: Optical properties and implementations in cancer diagnosis and photothermal therapy. Journal of Advanced Research, 1(1), 13-28.

Iyer, A. K., G. Khaled, *et al.,* (2006). "Exploiting the enhanced permeability and retention effect for tumor targeting." Drug discovery today 11(17-18), 812-818.

Jain, R. K., and Stylianopoulos, T. (2010). Delivering nanomedicine to solid tumors. Nature reviews. Clinical oncology, 7(11), 653-64.

Jana, N. R., L. Gearheart, *et al.,* (2001). "Wet chemical synthesis of high aspect ratio cylindrical gold nanorods." The Journal of Physical Chemistry B 105(19), 4065-4067.

Kang, B., Mackey, M. a, and El-Sayed, M. a. (2010). Nuclear targeting of gold nanoparticles in cancer cells induces DNA damage, causing cytokinesis arrest and apoptosis. Journal of the American Chemical Society, 132(5), 1517-9.

Kim, Y. and J. Yi (2008). "In-situ observation of deposition of gold nanoparticles on the amine-functionalized surface by open liquid-AFM." Korean Journal of Chemical Engineering 25(2), 383-385.

KOCKELMANN, W. and A. KIRFEL (2006). Neutron diffraction imaging of cultural heritage objects.

KoKKoli, E. (2011) Engineering Biomimetic Peptides for Targeted Drug Delivery, National Academies Press.

Lambert, J. B., H. F. Shurvell, *et al.,* (1998). Organic structural spectroscopy, Prentice Hall Upper Saddle River, NJ.

Lammers, T., W. Hennink, *et al.,* (2008). "Tumour-targeted nanomedicines: principles and practice." British journal of cancer 99(3), 392-397.

Lewinski, N., V. Colvin, *et al.,* (2008). "Cytotoxicity of nanoparticles." Small 4(1), 26-49.

Liu, X., M. Atwater, *et al.,* (2007). "Extinction coefficient of gold nanoparticles with different sizes and different capping ligands." Colloids and Surfaces B: Biointerfaces 58(1), 3-7.

Liu, Y., M. K. Shipton, *et al.,* (2007). "Synthesis, stability, and cellular internalization of gold nanoparticles containing mixed peptide-poly (ethylene glycol) monolayers." Analytical chemistry 79(6), 2221-2229.

Meng, F., Z. Zhong, *et al.,* (2009). "Stimuli-responsive polymersomes for programmed drug delivery." Biomacromolecules 10(2), 197-209.

Misra, R., and Sahoo, S. K. (2010). Intracellular trafficking of nuclear localization signal conjugated nanoparticles for cancer therapy. European Journal of Pharmaceutical Sciences:, 39(1-3), 152-63.

Moradei, O., C. R. Maroun, *et al.,* (2005). "Histone deacetylase inhibitors: latest developments, trends and prospects." Current Medicinal Chemistry-Anti-Cancer Agents 5(5), 529-560.

Murphy, C. J., A. M. Gole, *et al.,* (2008). "Gold nanoparticles in biology: beyond toxicity to cellular imaging." Accounts of chemical research 41(12), 1721-1730.

Nair, H. B., Sung, B., Yadav, V. R., Kannappan, R., Chaturvedi, M. M., and Aggarwal, B. B. (2010). Delivery of antiinflammatory nutraceuticals by nanoparticles for the prevention and treatment of cancer. Biochemical pharmacology, 80(12), 1833-1843.

Nelson, E. M., and Rothberg, L. J. (2011). Kinetics and mechanism of single-stranded DNA adsorption onto citrate-stabilized gold nanoparticles in colloidal solution. Langmuir: the ACS journal of surfaces and colloids, 27(5), 1770-7.

Nie, S. (2010). Understanding and overcoming major barriers in cancer nanomedicine. Nanomedicine (London, England), 5(4), 523-8.

Nie, S., Y. Xing, *et al.,* (2007). "Nanotechnology applications in cancer." Annu. Rev. Biomed. Eng. 9, 257-288.

Nistor, A. (2008). The Röntgen Radiation and its application in studies of advanced materials. Advanced Materials, 1-18.

Øie, S. (2004). Cellular drug delivery: principles and practice, Humana Pr Inc.

Palmeira-de-Oliveira, A., M. Ribeiro, *et al.,* (2010) "Anti-< i> Candida</i> Activity of a Chitosan Hydrogel: Mechanism of Action and Cytotoxicity Profile." Gynecologic and obstetric investigation 70(4), 322-327.

Pan, Y., S. Neuss, *et al.,* (2007). "Size Dependent Cytotoxicity of Gold Nanoparticles." Small 3(11), 1941-1949.

Park, K., S. Lee, *et al.,* (2009). "New generation of multifunctional nanoparticles for cancer imaging and therapy." Advanced Functional Materials 19(10), 1553-1566.

Pathak, P., V. Katiyar, *et al.,* (2007). "Cancer research-Nanoparticles, nanobiosensors and their use in cancer research." J. Nanotechnol. Online, 14.

Peer, D., J. M. Karp, *et al.,* (2007). "Nanocarriers as an emerging platform for cancer therapy." Nature Nanotechnology 2(12), 751-760.

Perera, F. H., F. J. Martinez-Vazquez, *et al.,* (2010) "Clarifying the effect of sintering conditions on the microstructure and mechanical properties of [beta]-tricalcium phosphate." Ceramics International 36(6), 1929-1935.

Philip, D. (2008). "Synthesis and spectroscopic characterization of gold nanoparticles." Spectrochimica Acta Part A: Molecular and Biomolecular Spectroscopy 71(1), 80-85.

Phillips, M. a, Gran, M. L., and Peppas, N. a. (2010). Targeted Nanodelivery of Drugs and Diagnostics. Nano today, 5(2), 143-159.

Polizzi, M. A., N. A. Stasko, *et al.,* (2007). "Water-soluble nitric oxide-releasing gold nanoparticles." Langmuir 23(9), 4938-4943.

Ponder, B. A. J. (2001). "Cancer genetics." Nature 411(6835), 336-341.

Raje, V. P., Morgado, P. I., Ribeiro, M. P., Correia, I. J., Bonifácio, V. D. B., Branco, P. S., *et al.,* (n.d.). Dual_On-off_and_Off-On_Fluorescent_Oligoaziridine_Probe_26.

Ribeiro, M. P., A. Espiga, *et al.,* (2009). "Development of a new chitosan hydrogel for wound dressing." Wound Repair and Regeneration 17(6), 817-824.

Rotello, V. M. (2008). "Advanced Drug Delivery Reviews Theme Issue:“Inorganic Nanoparticles in Drug Delivery”." Advanced drug delivery reviews 60(11), 1225.

Sahoo, S. K. and V. Labhasetwar (2003). "Nanotech approaches to drug delivery and imaging." Drug Discovery Today 8(24), 1112-1120.

Sarfati, G., T. Dvir, *et al.,* (2011) "Targeting of polymeric nanoparticles to lung metastases by surface-attachment of YIGSR peptide from laminin." Biomaterials 32(1), 152-161.

Schaeublin, N. M., L. K. Braydich-Stolle, *et al.,* (2011) "Surface charge of gold nanoparticles mediates mechanism of toxicity." Nanoscale.

Schleh, C., M. Semmler-Behnke, *et al.,* (2011) "Size and surface charge of gold nanoparticles determine absorption across intestinal barriers and accumulation in secondary target organs after oral administration." Nanotoxicology(0), 1-11.

Selvakannan, P., S. Mandal, *et al.,* (2003). "Capping of gold nanoparticles by the amino acid lysine renders them water-dispersible." Langmuir 19(8), 3545-3549.

Shan, J. and H. Tenhu (2007). "Recent advances in polymer protected gold nanoparticles: synthesis, properties and applications." Chemical Communications(44), 4580-4598.

Shenoy, D., W. Fu, *et al.,* (2006). "Surface functionalization of gold nanoparticles using hetero-bifunctional poly (ethylene glycol) spacer for intracellular tracking and delivery." International journal of nanomedicine 1(1), 51.

Stratton, M. R., P. J. Campbell, *et al.,* (2009). "The cancer genome." Nature 458(7239), 719-724.

Sugahara, K. N., T. Teesalu, *et al.,* (2009). "Tissue-penetrating delivery of compounds and nanoparticles into tumors." Cancer Cell 16(6), 510-520.

Sun, C., J. S. H. Lee, *et al.,* (2008). "Magnetic nanoparticles in MR imaging and drug delivery." Advanced drug delivery reviews 60(11), 1252-1265.

Sun, H., Hong, J., Meng, F., Gong, P., Yu, J., Xue, Y., *et al.,* (2006). Novel core-shell structure polyacrylamide-coated magnetic nanoparticles synthesized via photochemical polymerization. Surface and Coatings Technology, 201(1-2), 250-254.

Ting, A. H., K. M. McGarvey, *et al.,* (2006). "The cancer epigenome—components and functional correlates." Genes and development 20(23), 3215.

Van Gough, D. (2008). "Confocal Laser Scanning Microscopy."

Valeur, B., and Leray, I. (2000). Design principles of fluorescent molecular sensors for cation recognition. Coordination Chemistry Reviews, 205(1), 3-40.

Visvader, J. E. and G. J. Lindeman (2008). "Cancer stem cells in solid tumours: accumulating evidence and unresolved questions." Nature Reviews Cancer 8(10), 755-768.

Vogelstein, B. and K. W. Kinzler (2004). "Cancer genes and the pathways they control." Nature medicine 10(8), 789-799.

Wang, M., and Thanou, M. (2010). Targeting nanoparticles to cancer. Pharmacological Research, 62(2), 90-99.

Warenius, H. M., Galfre, G., Bleehen, N. M., and and Milstein, C. (1981). Attempted targeting of A monoclonal- antibody in a human-tumor xenograft system. European Journal Cancer Clinical Oncology, 17, 1009-1015.

Win, K. Y., & Feng, S.-S. (2005). Effects of particle size and surface coating on cellular uptake of polymeric nanoparticles for oral delivery of anticancer drugs. Biomaterials, 26(15), 2713-22.

Woof, J. M. and D. R. Burton (2004). "Human antibody–Fc receptor interactions illuminated by crystal structures." Nature Reviews Immunology 4(2), 89-99.

Yih, T. and M. Al Fandi (2006). "Engineered nanoparticles as precise drug delivery systems." Journal of cellular biochemistry 97(6), 1184-1190.

Zhang, L., F. Gu, *et al.*, (2007). "Nanoparticles in medicine: therapeutic applications and developments." Clinical Pharmacology and Therapeutics 83(5), 761-769.